UNIVERSITY OF HELSINKI REPORT SERIES IN PHYSICS

HU-P-D145

CHARACTERISATION OF CELLULOSE- AND LIGNIN-BASED MATERIALS USING X-RAY SCATTERING METHODS

Ulla Vainio

Division of X-Ray Physics
Department of Physical Sciences
Faculty of Science
University of Helsinki, Finland

ACADEMIC DISSERTATION

To be presented with the permission of
the Faculty of Science of the University of Helsinki,
for public criticism in the Auditorium E204
of the Department of Physical Sciences (Physicum),
Gustaf Hällströmin katu 2,
on June 20th, 2007, at 12 o'clock noon.

Helsinki 2007

Supervisor

Professor Ritva Serimaa

Department of Physical Siences
University of Helsinki
Helsinki, Finland

Reviewers

Professor Tapio Rantala

Institute of Physics
Tampere University of Technology
Tampere, Finland

Docent Anna-Kaisa Kontturi

Department of Chemical Technology
Helsinki University of Technology
Espoo, Finland

Opponent

Professor Adrian Rennie

Department of Physics
Uppsala University
Uppsala, Sweden

Report Series in Physics HU-P-D145
ISSN 0356-0961
ISBN 978-952-10-3255-4
ISBN 978-952-10-3256-1 (pdf-version)
http://ethesis.helsinki.fi/
Helsinki 2007
Helsinki University Printing House

Preface

The studies included in this thesis were carried out at the Division of X-ray Physics during years 2000 – 2007. I wish to thank Prof. Juhani Keinonen, the head of the Department of Physical Sciences, for providing me the opportunity to work at the department. I am very grateful also to the graduate school of the University of Helsinki and Vilho, Yrjö and Kalle Väisälä foundation for funding.

This thesis would not have been possible without the participation of a number of people. My gratest gratitude I owe to Prof. Timo Paakkari, who initially got me into the X-ray laboratory. A little later the name of the laboratory changed to Division of X-ray Physics and the next thing I know Prof. Ritva Serimaa — who later became my supervisor — was sending me to a synchrotron in Hamburg. She has helped, encouraged and given me opportunities that I had never dreamt of and for that I am indeed very grateful. I wish to thank Prof. Arto Annila for the stimulating discussions and for getting me the position at the graduate school. I thank Prof. Seppo Manninen and Prof. Keijo Hämäläinen for the encouraging and inspiring discussions and seminars as well as courses.

I wish thank my wonderful collaborators Prof. Nina Kotelnikova, Dr. Pekka Saranpää, Prof. Janne Laine, Prof. Liisa Kaarina Simola, Prof. Per Stenius, and the late Dr. Bo Hortling for samples and advise. Especially I would like to thank Dr. Natalia Maximova for the inspiring discussions and for the joyful collaboration. I am indebted to Prof. Jānis Grāvītis for the opportunity to work with lignins. Dr. Rolf Andreas Lauten I wish to thank for the inspiring collaboration regarding lignosulfonates. My thanks also to M.Sc. Thomas Kohout and M.Sc. Tiiu Elbra for magnetism studies and for the friendly attitude.

From the present and previous members of the Division of X-ray Physics I have to thank everybody for the warm atmosphere and funny jokes, and especially Dr. Mika Torkkeli, Dr. Seppo Andersson, Dr. Matti-Paavo Sarén, M.Sc. Marko Peura, M.Sc. Teemu Ikonen, M.Sc. Kari Pirkkalainen and M.Sc. Kaisa Kisko for their advise, support and collaboration.

During my thesis work I had an opportunity to study new materials at the University of Technology and I would like to thank Professor Olli Ikkala and Lic.Sc. Teija Laitinen for their collaboration and for letting me take part in their interesting studies concerning DNA. During the very end of this work I was able to learn a lot about anomalous small-angle x-ray scattering and synchrotron instrumentation from Dr. Günter Goerigk at the B1/JUSIFA beamline at HASYLAB, Hamburg. Many thanks for those precious moments. I also wish to thank all the people who visited the Division of X-ray Physics and with whom I had the pleasure to work with and from whom I have learnt so much during the past few years. There is not enough space to thank you all.

My deepest thanks also to my friends and family. Last but definitely not least I thank my mother Marjatta and my father Jukka for the always so kind support and especially for the warm meals and the philosophical discussions.

Helsinki, April 3th 2007

Ulla Vainio

U. Vainio : Characterisation of cellulose- and lignin-based materials using x-ray scattering methods, University of Helsinki, 2007, 46 pages + appendices. University of Helsinki, Report Series in Physics, HU-P-D145.

Abstract

The two most abundant polymers in nature are cellulose and lignin. They are the main components of cell walls of plants. The structure of the cell wall affects the properties of wood products. In wood fibres the cellulose chains spiral in the cell wall, and the helical angle between the direction of the chains and the longitudinal axis of the fibre, the microfibril angle, is one of the parameters that determine the strength of the fibre and the mechanical properties of wood. In this thesis the structure of Sitka spruce was studied using wide-angle x-ray scattering. The microfibril angle was observed to be large close to the pith of the tree but as a function of the annual ring the angle decreased. The annual rings at which the angle reached a small value depended strongly on the origin of the tree.

Cellulose is a widely used, environmentally compatible polymer. Recently, it was shown that metal containing cellulose composites could be used as catalysts. In this thesis the structure of cellulose composites containing copper and nickel was characterised using anomalous small-angle x-ray scattering. Metal ions were introduced to the solid cellulose support in an aqueous solution. Cellulose can reduce the metal ions but also more effective reducers were used.

Furthermore, lignin derivatives that are separated from the plant cell walls in pulping processes have many uses for example as dispersants. The structure of colloidal and dry lignin derivatives was characterised using small-angle and ultra-small angle x-ray scattering. In sulfite pulping lignin obtains sulfonate groups which make the so-obtained lignosulfonate a weak anionic polyelectrolyte that is soluble in water. The interactions of lignosulfonate particles were characterised in semidilute and concentrated solutions in different ionic strengths and in different temperatures using small-angle x-ray scattering.

Classification (INSPEC): A6110F, A6125H
Key Words: synchrotron radiation, SAXS, ASAXS, nanoparticle, x-ray diffraction, kraft lignin

Contents

Preface i

Abstract ii

Contents iii

List of Original Publications iv

Author's Contribution iv

1 Introduction 1

2 Aim of the thesis 2

3 Materials 3
- 3.1 Cellulose . . . 3
  - 3.1.1 Cellulose in wood . . . 4
  - 3.1.2 Cellulose as a support for nanoparticles . . . 5
- 3.2 Lignin . . . 5
  - 3.2.1 Lignin in wood . . . 5
  - 3.2.2 Lignin derivatives . . . 6

4 Theory and methods 6
- 4.1 X-ray methods . . . 6
- 4.2 Measurement geometries . . . 8
  - 4.2.1 Symmetrical reflection and transmission . . . 8
  - 4.2.2 Perpendicular transmission . . . 9
- 4.3 Wide-angle x-ray scattering . . . 9
- 4.4 Small-angle x-ray scattering . . . 10
  - 4.4.1 Scattering from particles without interparticle interactions . . . 11
  - 4.4.2 Scattering from particles with interparticle interactions taken into account . . . 14
  - 4.4.3 Power-law scattering . . . 16
- 4.5 Anomalous small-angle x-ray scattering . . . 17
- 4.6 X-ray absorption . . . 20

5 Results and discussion 21
- 5.1 Cellulose-based materials . . . 21
  - 5.1.1 Coordination of metal ions onto cellulose . . . 23
  - 5.1.2 Thermal expansion of cellulose . . . 24
  - 5.1.3 Cellulose in wood . . . 27
- 5.2 Lignin-based materials . . . 28

6 Future aspects 31

References 33

List of original publications

This thesis consists of an introductory part followed by five publications, referred in the text as Papers **I** – **V**.

I Vainio U, Andersson S, Serimaa R, Paakkari T, Saranpää P, Treacy M, and Evertsen J. *Variation of microfibril angle between four provenances of Sitka Spruce (*Picea sitchensis *[Bong.] Carr.).* Plant Biology **4** (2002), 27 – 33.

II Vainio U, Pirkkalainen K, Kisko K, Goerigk G, Kotelnikova NE, and Serimaa R. *Copper and copper oxide nanoparticles in a cellulose support studied using anomalous small-angle x-ray scattering.* European Physical Journal D **42** (2007), 92 – 101.

III Pirkkalainen K, Vainio U, Kisko K, Elbra T, Kohout T, Kotelnikova NE, and Serimaa R. *Structure of nickel nanoparticles in a microcrystalline cellulose matrix studied using anomalous small-angle x-ray scattering.* Journal of Applied Crystallography **40** (2007), s489 – s494.

IV Vainio U, Maximova N, Hortling B, Laine J, Stenius P, Simola LK, Gravitis J, and Serimaa R. *Morphology of dry lignins and size and shape of dissolved kraft lignin particles by x-ray scattering.* Langmuir **20** (2004), 9736 – 9744.

V Vainio U, Lauten RA, and Serimaa R. *Structural and rheological properties of aqueous lignosulfonate solutions.* Submitted to European Physical Journal E (2007).

Articles **I** – **V** are reprinted with permissions from the publishers.

Author's Contribution

In Paper **I** the author performed all the x-ray measurements and the analysis except for crystallinity and crystallite size determination, and participated in writing of the paper. In Paper **II** the author participated in the ASAXS measurements, analysed the results, participated in the analysis of XRD measurements and wrote most of the paper. In Paper **III** the author participated in the ASAXS measurements, but not in the analysis, measured and analysed the XRD patterns, participated in VSM measurements and wrote the paper expect for the ASAXS part. In Paper **IV** the author participated in writing of the paper and the x-ray measurements and analysed the results. In Paper **V** the author carried out all experimental work and analysis concerning x-ray measurements and wrote most of the paper. The author did not participate in synthesis or making of any of the samples presented in any of the papers.

1 Introduction

In the past few years the climate change has been given a lot of media visibility. At the same time the energy consumption increases world wide and simultaneously a growing number of people in the developing countries will join the consumer society. The only solution seems to be sustainable development (Eissen *et al.*, 2002). Renewable resources and more efficient recycling are needed. Previously the attitude towards the left-over products from industries was well described by the use of word 'waste liquor' to mean the spent liquor of pulp mills. Nowadays both money and sustainability play a key role in turning the 'waste' into something useful in every industry. From the spent liquor a side-product, lignin, can be extracted. In different pulping processes the lignin, which is the most abundant natural aromatic polymer on Earth, is separated in different forms. At the moment it is vastly under-utilised. (Lora and Glasser, 2002)

Currently the most used pulping process is kraft pulping and lignin obtained from that process is called kraft lignin. The less used sulfite pulping process produces another lignin product called lignosulfonate. The main difference between these products is at first sight the different solubilities to water. While lignosulfonate is completely soluble in aqueous solutions kraft lignin is soluble only in certain conditions.

The production of solid lignosulfonate is 1 million tons per year (Gosselink *et al.*, 2004). The annual production of kraft lignin is many times larger than that of lignosulfonate, but traditionally the lignins are used as a fuel in the recovery furnaces of the pulp mills (Li *et al.*, 1997). Due to the efficiency of the modern pulp mills the mills no longer can spend all the energy they gain from the extracted lignins and already since the 1970s other uses for lignin have been developed besides the use as a fuel. This has lead to the need to characterise lignin and its derivatives more completely. (Dong and Fricke, 1995) In this thesis an attempt was made to describe the morphology and the interactions of dissolved lignin particles as this is the most natural state of the end products of lignin. The nanometre scale structure of dry lignin was also characterised.

For more than 50 years lignosulfonate has been used as a dispersant and an adhesive for various applications even though at the beginning the underlying mechanisms leading to its good properties as a dispersant were unknown (Gardon and Mason, 1955). Sulfonated lignin derivatives from the sulfite pulping process have been used as binders and dispersants in various products such as concrete (Gundersen *et al.*, 2001; Ouyang *et al.*, 2006) and as dust suppressants on roads. Recently, it was found that a sulfate lignin derivative inhibits a common herpes simplex virus from entering cells and thus even some medical applications might be possible in the future for the lignins (Raghuraman *et al.*, 2005). The extracted lignins could be used as starting materials for various molecules that are nowadays produced from fossil resources. They are also regarded as a renewable energy source. (Pye, 2005; Petrus and Noordermeer, 2005) New products are being developed from lignin and recently lignin-based thermoplastics have been prepared from kraft lignin (Li *et al.*, 1997). Although lignin and cellulose are marketed as renewable and sustainable choices for raw materials, some critical remarks about the eco-efficiency of biopolymers and especially lignin have also been brought up (Scott and Wiles, 2001).

The most abundant polymer in nature is cellulose. The use of cellulose has a long history. Without the knowledge of its structure cellulose has been used already for centuries in various fields, for example as a raw material for paper and clothes. In 1838 the molecular formula of cellulose was determined to be $C_6H_{10}O_8$ by Anselme Payen, but the most astonishing discovery was yet to come 80 years later. The polymeric state of cellulose was

observed by Hermann Staudinger in his pioneering work in 1920. Discovery of the covalent bonding of the D-glucose units gave evidence that cellulose was a very large molecule, a *macromolecule*. This was the starting point of polymer science. (Klemm *et al.*, 2005) The structure of cellulose has been well characterised and an increasing number of studies are related to the use of cellulose as a starting material for novel applications. In this thesis the structure of metal containing cellulose composites was characterised in order to have a better understanding of the effect of reaction conditions on the structure of these materials.

Even though these new materials are being developed, wood itself remains a popular raw material for various products in construction and furniture industries. For these industries the quality and strength of the starting material is important. The structure of wood cells determines the strength of the fibres and finally the feasibility of the end product. In this thesis the structure of wood cells of Sitka spruce trees was studied. The seeds of the fast growing spruce species were imported from different locations of the west coast of North America to Ireland and grown in similar conditions. After the trees were felled and samples were taken, the structure of the samples was studied as a function of the annual ring using x-ray diffraction. Significant differences were noticed in the structure depending on the origin of the seed.

In this thesis x-ray scattering methods were used to study the structure of cellulose- and lignin-based materials. X-ray scattering is an excellent method for the characterisation of the structure of materials from the atomic scale up to several hundred nanometres.

2 Aim of the thesis

This thesis presents some methods by which wood, cellulose and lignin can be characterised using x rays. In order to gain better understanding of the structure and the behaviour of the studied cellulose- and lignin-based materials these materials need to be characterised in different conditions.

In Paper **I** the structure of Sitka spruce was characterised in the nanometre level. The strength of wood cells is partially based on the angle in which the cellulose microfibrils spiral in the wood cell wall. The microfibril angle is known to be heritable to some degree (Myszewski *et al.* (2004) and references therein). In Paper **I** it was shown that the microfibril angle depends on the origin of the Sitka spruce seed.

In papers **II** and **III** porous microcrystalline cellulose obtained from cotton was used to study the interactions of metal ions with the cellulose fibres. The aim was to understand what kind of structures the metal atoms form in the fibre and on the fibre. In the summary part of the thesis the thermal expansion of the cellulose crystallites in the samples containing the metal nanoparticles has been examined in more detail.

In papers **IV** and **V** the lignin removed from the wood cells by using different separation methods was studied in order to establish a better understanding of the shape of the lignin particles in solution as well as their self-association. When the lignins are dried, their morphology depends on the drying process and the shape and interactions of the lignin particles. One of the objectives was to study whether the fractal model could be applied to dried lignins.

3 Materials

Cellulose microfibrils give wood cells their good mechanical properties while hemicelluloses and lignin act as a "glue" in between the cellulose crystallites. The structure of wood and its components has been described in several textbooks (Sjöström, 1993; Sarkanen and Ludwig, 1971). X-ray scattering methods have a long history related to the characterisation of cellulose fibres and already in 1932 cellulose fibres were observed to give small-angle x-ray scattering (Guinier and Fournet, 1955, p. 179). The complex structure of wood has continued to interest scientists and today the x-ray scattering patterns are better understood and give very detailed information about the structure of wood (Sarén, 2006; Andersson, 2007).

3.1 Cellulose

Cellulose is a linear homopolysaccharide that is composed of β-D-glucopyranose units which are linked together by $(1 \rightarrow 4)$-glycosidic bonds. (Sjöström, 1993, pp. 54 – 55) The chemical structure of the cellulose monomer and that of the cellulose chain are presented in Figure 1.

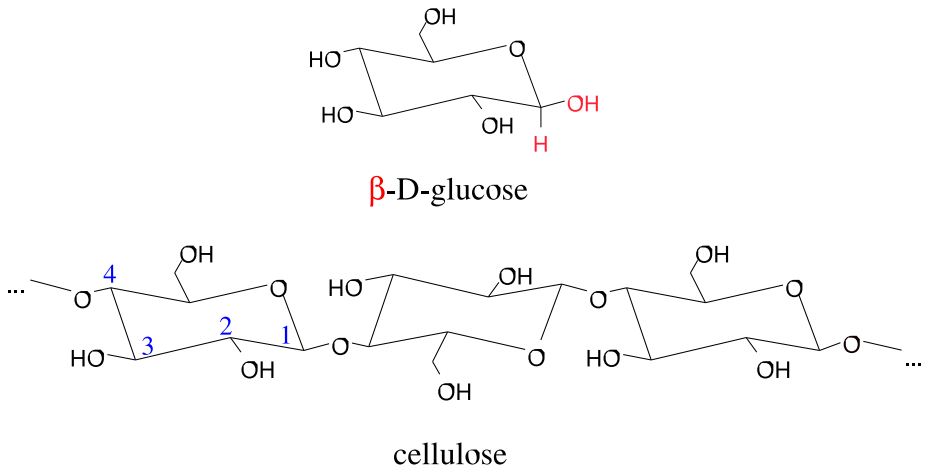


Figure 1: The glucose-unit and the cellulose chain.

Cellulose can crystallise or be crystallised in many different polymorphic forms of which currently are known Iα, Iβ, II, $\mathrm{III_I}$, $\mathrm{III_{II}}$, $\mathrm{IV_I}$, and $\mathrm{IV_{II}}$ (Zugenmaier, 2001). The allomorph $\mathrm{IV_I}$, however, is likely to be falsely classified, since recent studies have shown that it might be just a less crystalline form of cellulose I (Wada *et al.*, 2004b). The unit cells of the allomorphs have been identified to have either a triclinic space group P1 (Iα, $\mathrm{IV_I}$, and $\mathrm{IV_{II}}$) or a monoclinic space group $\mathrm{P2_1}$ (Iβ, II, $\mathrm{III_I}$). All of the allomorphs have the polymer chains aligned along the crystallographic c-axis so that the unit cell length of each allomorph is about $10.3 - 10.4$ Å in length in the direction of the chains. (Zugenmaier, 2001) In each allomorph the chains are also organised into sheets. Each sheet is composed of cellulose chains that are hydrogen bonded to the neighbouring chains, but the bonding between the sheets is different in the different allomorphs. The main difference in the native structures of cellulose, Iα and Iβ, is the relative displacement of the cellulose sheets in the c-direction. The stacked sheets are weakly bonded by C–H$\cdots$O bonds and van der Waals interactions

in the native celluloses (Nishiyama *et al.*, 2002), while in celluloses II and III_I the sheets are inter-connected through hydrogen bonds. (Wada *et al.*, 2004a)

When cellulose I is treated with alkali the crystalline lattice is disturbed by swelling. The crystalline structure of the cellulose after washing away the alkali is different from cellulose I and is called cellulose II (Preston, 1974, pp. 140 – 141).

3.1.1 Cellulose in wood

The cellulose crystallites are wound helically in the cell walls of wood fibres. This helical angle is parametrised by an angle called the microfibril angle (MFA) as shown in Figure 2. Two of the polymorphic forms of cellulose are found in nature in the plant cell walls. The Iα and Iβ allomorphs have been found even along a single microfibril of green alga *Microdictyon tenuius*. By thermal treatment the Iα allomorph can be transformed to Iβ. (Sugiyama *et al.*, 1991) The ratio of Iα to Iβ varies between plant species in such a way that Iα is mostly found in the cell walls of some algae and in bacterial cellulose, while Iβ is more common in higher plants such as trees (Atalla and VanderHart, 1984; Nishiyama *et al.*, 2003).

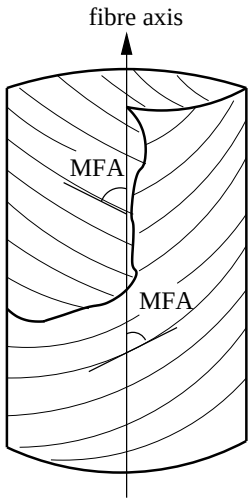


Figure 2: A schematic view of a wood fibre (the cylinder) and the cellulose chains that circle around the fibre in an angle called the microfibril angle (MFA).

In this study the MFA distribution of Sitka spruce (*Picea sitchensis* [Bong.] *Carr.*) from four different provenance locations in North America was studied. Due to its excellent growth rate it has also been imported to Europe. To examine the capability of Sitka spruce to adapt to the conditions in Ireland, Sitka spruce seeds from different locations in North America were collected. From each provenance location 20 – 30 seeds were collected and grown in a nursery in Ireland and in the spring of 1976 the transplants were planted in 2×2 m spacing into similar environmental conditions. (Thompson, 2006; Treacy *et al.*, 2000) The trees were felled in 1996 and the microfibril angle as a function of the annual ring was studied in the case of four provenances: California (Crescent City), Oregon (Brookings), Queen Charlotte Islands (Copper Creek), and Washington (Nasselle). Samples from 3 – 4 trees per provenance were studied using x-ray diffraction (Paper **I**).

3.1.2 Cellulose as a support for nanoparticles

Microcrystalline cellulose (MCC) prepared by mild acid hydrolysis from cotton was used as a support for copper and nickel nanoparticles (Papers **II** and **III**). The metal ions were introduced in an aqueous solution to the solid cellulose matrix and reduced with either the cellulose or one of the stronger reducers: sodium borohydride ($NaBH_4$), potassium hypophosphite ($KH_2PO_2 \cdot H_2O$) or hydrazine sulfate ($N_2H_4 \cdot H_2SO_4$). In the synthesis of the nanoparticles the molar ratio between copper ions Cu^{2+} or nickel ions Ni^{2+} and microcrystalline cellulose monomers was varied. In the synthesis of some samples ammonium hydrate ($NH_3 \cdot H_2O$) or glycerol was added to the aqueous medium before reduction.

3.2 Lignin

3.2.1 Lignin in wood

While cellulose is a completely linear and structurally well defined polymer, lignin is a branched polymer and its structure cannot be described by a simple structural formula. In fact, lignin is amorphous and its chemical composition varies from plant to plant and may even be different at different parts of the plant. An oriented structure of lignin has also been proposed to be present in the cell walls in such a way that the lignin would be ordered analogous to the cell wall polysaccharides (Åkerholm and Salmén, 2003). For example, it has been shown by ozonation analysis that the chemical structure of lignin associated closely to carbohydrates is different from that of the major part of lignin (Aimi *et al.*, 2004). In Figure 3 the structure of the most important structural unit of a lignin polymer is shown.

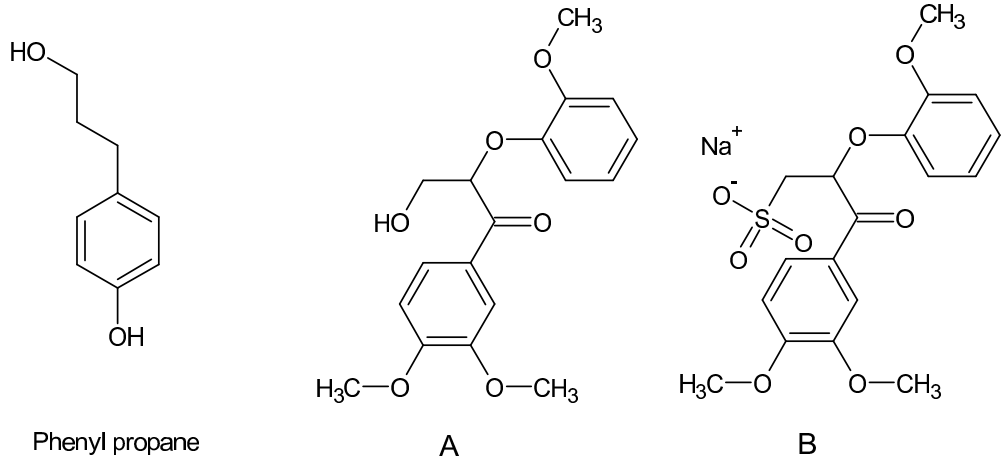


Figure 3: On the left is the basic structural unit of lignin which is a branched polymer (Adler, 1968) and on the right a model compound of lignin (A) and the model compound in sodium salt form after acid sulfite pulping (B) (Gellerstedt, 1976).

It has been suggested that lignin is chemically bonded to cellulose and xylan in the cell walls (Furano *et al.*, 2006) and that the carbohydrates are linked to lignin through benzyl ether linkages (Lawoko *et al.*, 2006). This means that differently prepared lignins contain different amounts of carbohydrate impurities.

In Paper **IV** dried lignins from different sources were studied in order to compare the supramolecular structure of different lignins of which some are regarded to be close

the natural state of lignin. Especially the released suspension culture lignin has been described as being very natural as it is released from cell walls without mechanical or chemical treatments (Simola *et al.*, 1992).

Even though chemical and mechanical separation of lignin from wood definitely alters the structure of the molecules, it is still possible that the smallest of the separated lignin molecules have the same morphology as the lignin in the cell walls. The morphologies of two types of low molar mass lignin derivatives obtained by different pulping methods were studied in aqueous solutions in Papers **IV** and **V**.

3.2.2 Lignin derivatives

Different lignin derivatives are obtained from the spent liquors of pulp mills as a side product of the pulping process. The spent liquor, called "black liquor" due to its dark colour, contains mostly lignin but also sugars from degraded hemicellulose and cellulose and salts (Nadif *et al.*, 2002).

Kraft pulping (sulfate pulping) is globally the most used method of pulping (Chakar and Ragauskas, 2004). The dry substance in the black liquor of kraft pulps is high, about 15 – 20 % (Wallberg and Jönson, 2006). The colloidal properties of kraft lignin are therefore of practical interest. It is no wonder that there exists many studies that deal with these properties as well as the association of the lignin macromolecules (Maximova, 2004). Kraft lignin was studied also in Paper **IV**.

Another interesting lignin derivative is the lignosulfonate (also called ligninsulfonate, sulfonated lignin etc.) which is a negatively charged polyelectrolyte that is extracted from the spent liquors of sulfite pulp mills. During the sulfite pulping process lignin is modified into lignosulfonate by addition of sulfonate groups (SO_3^-) which make the lignin soluble in water (Fig. 3). The colloidal structure and interactions of lignosulfonate macromolecules were studied in Paper **V**.

4 Theory and methods

Several studies included in this thesis deal with colloidal dispersions (Hunter, 1991, 1992). The structures of the studied systems were characterised by using x-ray scattering and x-ray absorption methods.

4.1 X-ray methods

The principle in the used x-ray scattering methods is the detection of the intensity of elastically scattered x rays from the sample when the sample is being hit by a monochromatic beam of x rays. Different measurement geometries can be used. In this thesis the most common geometries of *symmetrical reflection*, *symmetrical transmission* and *perpendicular transmission* were used.

Due to the extensive use of these methods in physics, chemistry and biology, it is sometimes forgotten that the analysis of the x-ray scattering patterns is fundamentally based on a number of approximations. First of all, the scattering must be elastic which means that the energy of the scattered radiation is exactly the same as that of the incident radiation.

In addition to the elastic scattering other processes such as Compton scattering, scattering from plasmons, Raman and resonant Raman scattering, fluorescence and thermal diffuse scattering (TDS) can give contribution to the observed intensity. (Cowan, 1994; Wilson, 1995, pp. 570 – 578) In the small-angle x-ray scattering (SAXS) studies of this thesis the other scattering processes besides the elastic scattering have been considered to give a flat background that can be subtracted from the scattered intensity. Now we shall justify why removal of the other components is possible by such a simple procedure and why it does not cause a major error in the analysis of the elastically scattered intensity.

The energy change of the photon in the Compton scattering process depends on the energy of the incident radiation and on the angle to which the photon is scattered. At small scattering angles the change in the energy of the photon is very small and thus experimental removal of this scattering would be very time consuming and unrealistic. Luckily, the intensity of the Compton scattering is small at small scattering angles because the energy change is so small that scattering cannot occur from core electrons; only the most loosely bound electrons will contribute to the Compton scattering at the small scattering angles. The TDS is inelastic scattering from collective lattice vibrations, the phonons. In crystalline materials the thermal diffuse scattering is centred at the same angles as the diffraction spots. The other inelastic processes give a smooth background also in the case of crystalline materials.

The resonant Raman scattering and the fluorescence are mainly important when the energy E of the incoming photons is near to the energy E_{edge} of an absorption edge of an element ($0.9 < E/E_{edge} < 1.1$). These processes can cause a flat energy dependent background to the x-ray scattering intensity at small scattering angles. Fluorescence is the process where the incident x rays excite electrons from their ground levels. When these ground states are filled with electrons from higher energy levels the atoms emit light (fluorescence) which has a smaller energy than the incident x rays. The intensity of the resonant Raman scattering exceeds that of the Compton scattering at photon energies below the absorption edge while after the edge the fluorescence is dominant. The scattering from plasmons and the Raman scattering are unlikely to give a strong contribution to the background. In conclusion, usually at the small-angle scattering region the contributions from all these non-elastic processes will be small compared to the elastic scattering but the their proportion of the total scattering intensity depends on the energy of the incident radiation and on the composition of the sample.

Once the significant contribution arising from the other processes has been removed from the detected intensity, the elastically scattered intensity can be further analysed in order to get information on the structure of the sample. In this thesis all of the samples could be analysed by using the results of the *kinematical theory*. The use of the kinematical theory relies on two approximations (Azároff *et al.*, 1974, pp. 70 – 71). Firstly, the intensity of the radiation scattered by the sample must be very small compared to the intensity of the radiation passing through the sample *i.e.* the incident beam. Secondly, both the incident radiation hitting the sample and the scattered radiation observed on the detector can be approximated as plane waves (Fraunhofer diffraction).

The first approximation means that multiple scattering events are neglected. Corrections can be made to take the multiple scattering into account but in this study all such corrections were neglected and it was assumed that the multiple scattering was small at small scattering angles. This can be checked by using samples of different thicknesses. For polymer samples the two approximations are satisfied at small scattering angles because

of the measurement setup and the used wavelength. The breaking of either the first or the second approximation would alter the shape of diffraction maxima.

By using the assumptions of the kinematical theory it is possible to calculate the scattered amplitude from the atomic coordinates of the sample by a Fourier transform. However, we are troubled with the fact that we observe intensity, which is the amplitude squared. Therefore we cannot make an inverse Fourier transform to directly retrieve the positions of the atoms because the phase information is lost in the squaring. For single crystals some methods exist by which this so called phase problem can be by-passed.

In the publications of this thesis we are not dealing with single crystals but with soft matter, which is mostly amorphous. In this case the phase problem cannot be tackled due to the lack of a long range order in the sample. This will result in a number of approximations and ways to interpret the scattering patterns.

4.2 Measurement geometries

4.2.1 Symmetrical reflection and transmission

Symmetrical reflection and symmetrical transmission methods are typically used in scattering studies where excellent accuracy of the scattering angle 2θ is required. A scheme of a $\theta - 2\theta$ diffractometer is shown in Figure 4 in the reflection geometry. The transmission geometry is otherwise the same, but the sample is rotated 90 degrees in the plane of the goniometer. The orientation of the crystalline scatterers in the sample can be measured by keeping the angle 2θ constant at the position of a reflection and by varying the azimuth angle χ so that the sample is rotated along the axis normal to the sample surface.

Corrections for absorption and air scattering were done to the intensities according to the procedures described in Klug and Alexander (1974) when the intensity as a function of the scattering angle 2θ was of interest. For the orientation measurements scattering angle dependent corrections were not needed.

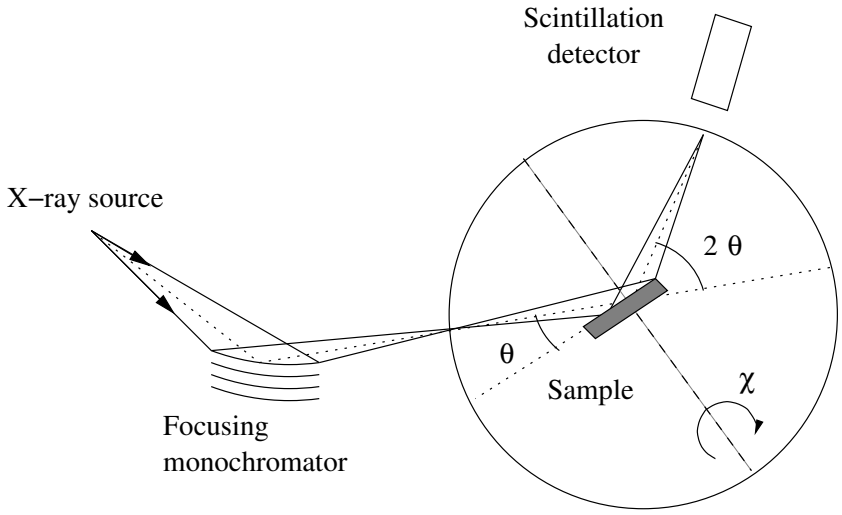


Figure 4: A schematic view of the reflection geometry of a θ-2θ diffractometer.

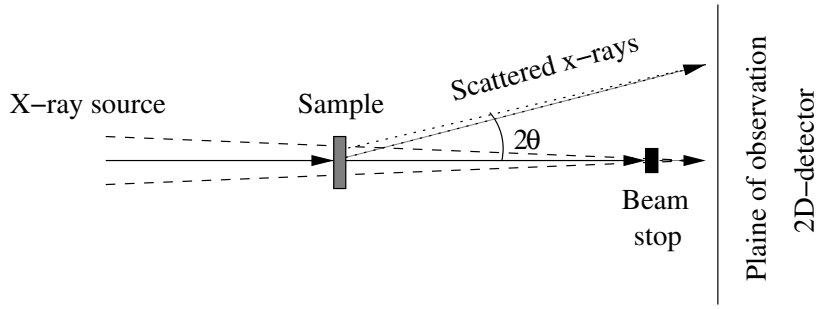


Figure 5: A schematic view of the perpendicular transmission geometry. The monochromatic x rays can either be focused on the detector or collimated.

4.2.2 Perpendicular transmission

The perpendicular transmission geometry (Fig. 5) is less accurate than the symmetrical reflection geometry but it has some advantages which make it especially suitable for the study of soft materials. Usually the amount of material to be studied is limited. In the perpendicular transmission geometry a much smaller sample is needed than in the symmetrical transmission and reflection geometries. With a 2D-detector the orientation of the scatterers in the plane of the sample (normal to the beam) is easily revealed by a single measurement because the azimuth angles are detected simultaneously. Soft carbon based materials scatter x rays weakly in the typical x-ray energies. If short measurement times are needed, it is thus more economical to detect the intensity at each scattering angle simultaneously using a 2D detector instead of scanning step-by-step over 2θ and χ. The temperature control of the sample is easier when the sample size is small and a close contact to the heat source is possible. In symmetrical transmission and reflection geometries this requires more elaborate solutions than in the perpendicular transmission geometry. This makes perpendicular transmission geometry an excellent method for the study of temperature induced changes in materials.

Corrections need to be done to the intensity like in the case of the symmetrical methods. The absorption of the sample must be corrected for and the scattering from air must be subtracted. The beginning of the scattering curve of weak scatterers turns down sometimes due to inaccurate subtraction of the background when the scattering from air is very intense. Care was taken in each experiment to avoid such a situation, but nevertheless it sometimes occurred.

4.3 Wide-angle x-ray scattering

The term x-ray diffraction (XRD) is commonly used to describe experiments made using either the symmetrical transmission or reflection geometry. Strictly speaking diffraction refers to a scattering process from a crystalline sample and therefore the term x-ray scattering should be preferred when the studied samples are not crystalline. Therefore, the term wide-angle x-ray scattering (WAXS) was used in some cases to cover the scattering from both crystalline and amorphous samples.

4.4 Small-angle x-ray scattering

Small-angle x-ray scattering (SAXS) is a technique which gives information on structures of size from about 1 nm to about 100 nm. Ultra-small angle x-ray scattering (USAXS) can be used to study structures whose size goes up to micrometres. The small-angle scattering method is at its best when changes in the sample are monitored as a function of some external parameter such as concentration, pH, temperature, pressure, or moisture. The basics of SAXS are well covered in the literature. There are textbooks about small-angle scattering alone (Glatter and Kratky, 1982; Feigin and Svergun, 1987; Guinier and Fournet, 1955), and many general x-ray scattering books like Guinier (1994) have a section on small-angle scattering.

Figure 6 shows a simulated scattering intensity from a crystalline platelet. In the figure and throughout the entire thesis the length of the scattering vector is defined

$$q = \frac{4\pi \sin\theta}{\lambda}, \tag{1}$$

where θ is half of the scattering angle and λ is the wavelength of the radiation. The so called Bragg distance is calculated as $d_{hkl} = 2\pi/q$. For a crystalline material it directly tells the distance between two crystalline planes when q is the position of the diffraction maximum. Calibration of the q-scale in a SAXS experiment is usually done with Silver Behenate (Huang *et al.*, 1993). Instead of the notation q some people prefer to call the length of the scattering vector k, h or Q and a notation commonly used especially in the older literature is s which is defined $q/(2\pi)$. This might be confusing sometimes. In any case the use of the scattering vector is more convenient than the use of the scattering angle 2θ because q does not depend on the wavelength.

Figure 6 illustrates the arbitrarily drawn distinction between small- and wide-angle x-ray scattering and how the Guinier and power-law regions in the small-angle scattering region are related to each other. For the crystalline platelet we observe reflections at the wide-angle scattering region. The shape and width of the reflections are connected to the shape and size of the crystallites. An estimate for the size of the crystallite in the direction perpendicular to the scattering planes can be determined from the width of the reflection using the Scherrer formula (Guinier, 1994). For amorphous samples only SAXS gives information on the shape and size of the particles because there are no crystalline reflections. It can be thought that the small-angle scattering is actually the reflection 00 (or in the case of three dimensional particles the reflection 000) because the shape of the SAXS peak located at $q = 0$ depends similarly on the shape and size of the particle.

Scattering intensity is defined as the absolute square of the scattering amplitude. The simplest way to calculate the scattering intensity $I(q)$ of a powder sample is to use the Debye formula (Guinier, 1994, p. 49)

$$I(q) = \sum_{n=1}^{N} \sum_{m=1}^{N} f_n f_m \frac{\sin(q x_{nm})}{q x_{nm}}, \tag{2}$$

where f_n and f_m are the scattering factors of point-like scattering units n and m which are located at a distance x_{nm} from each other. The total number of points is N. This formula is particularly useful when one needs to test ideas and analytical formulae. Since the distinction between small- and wide-angle scattering is artificial, the Debye formula can be applied in both methods. However, the computing time rapidly increases with the

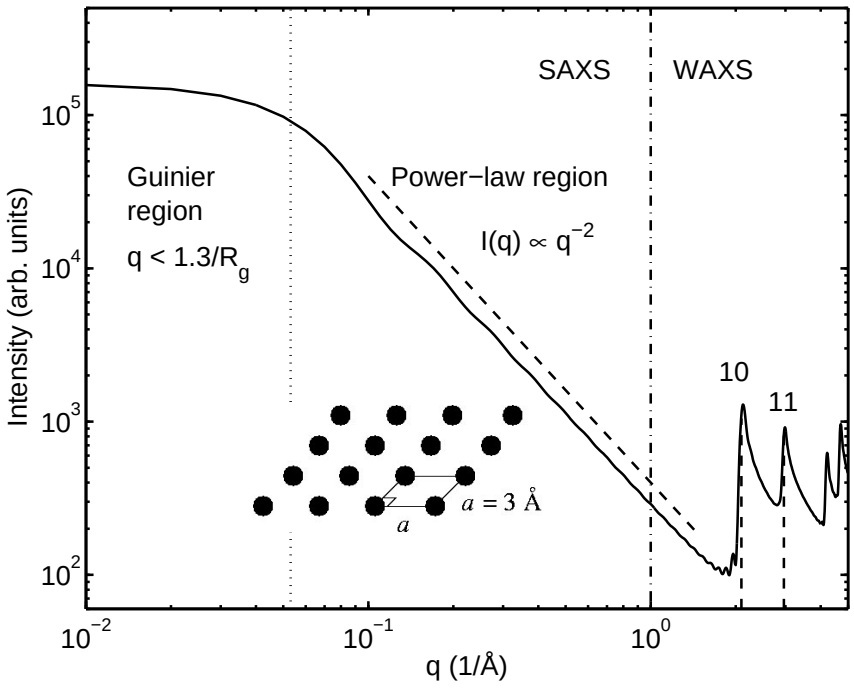


Figure 6: Calculated scattering from a 6 nm × 6 nm platelet (radius of gyration R_g = 24.5 Å) of points using the Debye formula. The different regions of interest are separated by vertical lines. The inset shows a part of the platelet. Data from Vainio *et al.* (2006).

number of points used, so it is not suited for all purposes and therefore we shall next introduce a few analytical equations that explain from which components the scattering intensities are composed of.

The intensity $I(q)$ can be transformed onto absolute intensity scale by using a calibration sample of known intensity (Orthaber *et al.*, 2000). The absolute intensity is given by the differential scattering cross section $\mathrm{d}\Sigma/\mathrm{d}\Omega$ which has units cm^{-1}. Most of the equations we will use do not require the absolute intensity normalisation, but whenever it is needed the formula is given in absolute intensity units. If the scattering intensity is not normalised, the shape of the intensity curve is more important in those cases.

4.4.1 Scattering from particles without interparticle interactions

In the theory of small-angle scattering we often make the assumption that the studied particles are in random orientations and do not interact with each other. This lack of interparticle interaction is very similar to the one met in the theory of ideal gas. If there is a certain distance that the particles prefer to have with respect to each other, a maximum is observed in the scattering pattern. This preferred distance between particles occurs for example in solutions of highly charged macromolecules as they are unable to approach very close to each other due to the electrostatic repulsion. Next we will consider systems in which the interparticle interactions can be neglected.

A solution of monodisperse spherical particles is the most simple case that can be studied. The differential cross section $\mathrm{d}\Sigma/\mathrm{d}\Omega$ of N monodisperse spheres in an irradiated

volume V can be expressed (*e.g.* Pedersen (1997); Shen *et al.* (1988); Ottewill *et al.* (2003))

$$\begin{aligned} \frac{\mathrm{d}\Sigma}{\mathrm{d}\Omega} &= \frac{N}{V} V_p^2 (\overline{\rho} - \rho_s)^2 P(q) S(q) \\ &= \phi V_p (\overline{\rho} - \rho_s)^2 P(q) S(q), \end{aligned} \tag{3}$$

where V_p is the volume of one particle, $\overline{\rho}$ is the average electron density of the particle, ρ_s is the electron density of the solvent and ϕ is the volume fraction of the solid material. The form factor $P(q)$ is normalised to one at $q = 0$. Its shape depends only on the shape of the particle. The interparticle structure factor $S(q)$ is equal to 1 for non-interacting particles.

In the case of globular non-interacting particles the beginning of the scattering intensity curve is independent of the shape of the particles. For monodisperse globular particles the Guinier approximation can be used near $q = 0$ to give the radius of gyration R_g. The approximation is written as (Guinier, 1994, p. 329)

$$I(q) \propto \exp\left(-\frac{q^2 R_g^2}{3}\right) \tag{4}$$

and is valid at $qR_g < 1.3$ (Svergun and Koch, 2003). The R_g is obtained by fitting a straight line to the Guinier plot (q^2,$\ln I(q)$).

While the Guinier approximation applies near $q = 0$ for the non-interacting particles, the so called Porod law $I(q) \propto q^{-4}$ can be shown to apply at large values of q for globular particles even in interacting systems and moreover in two-phase systems (Glatter and Kratky, 1982, pp. 29 – 32, 46 – 47). Using the differential cross section we can write for the particles in the irradiated volume V the Porod constant in the form (Spalla *et al.*, 2003)

$$\begin{aligned} \lim_{q\to\infty} q^4 \frac{\mathrm{d}\Sigma}{\mathrm{d}\Omega} &= 2\pi \frac{N}{V} (\overline{\rho} - \rho_s)^2 S \\ &= 2\pi\phi (\overline{\rho} - \rho_s)^2 \frac{S}{V_p}, \end{aligned} \tag{5}$$

where S/V_p is the surface-to-volume ratio of one particle. If the scattering intensity curve at the small-angle scattering region follows the Porod law, it is possible to get information about the size and shape of the particle by using the Porod constant since the surface-to-volume ratio of the particle directly depends on the size and shape of the particle.

Another way to study the shape of the particle is to compute the distance distribution function $p(R)$ which is obtained from the scattering intensity by a Fourier transform (Glatter and Kratky, 1982, pp. 20 – 22, 130 – 131)

$$p(R) = \frac{R^2}{2\pi^2} \int_0^\infty I(q) \frac{\sin(qR)}{qR} q^2 \mathrm{d}q, \tag{6}$$

where R is a distance between two points in the particle. The shape of the function is determined by the shape of the particle and it can be calculated analytically for differently shaped particles. The $p(R)$ function is effectively the autocorrelation function of the particle times the distance R squared. Because R is a distance between two points in the particle, the function goes to zero at some maximum distance R_{max} which is the maximum diameter of the particle. In order to use Equation 6 it is necessary to extrapolate the intensity curve to $q \to 0$ and $q \to \infty$. Typically the beginning of the scattering curve near

$q = 0$ is approximated by the Guinier law and the end is approximated with the Porod law. In this extrapolation the absolute intensity units are not needed.

In many cases we are interested in finding the size distribution of a set of particles in solution or in another medium. By neglecting the interparticle interference effects we may write the intensity scattered from a polydisperse set of spheres as (Pedersen, 1997)

$$I(q) = \sum_{n=1}^{N} \nu(R_n) V_p(R_n)^2 P_{\mathrm{sph}}(q, R_n). \tag{7}$$

Here $\nu(R_n)$ is the fraction (or number size distribution) of spheres of radius R_n in the sample while the form factor of a sphere of radius R_n is (Guinier, 1994, pp. 322 – 324)

$$P_{\mathrm{sph}}(q, R_n) = \frac{9(\sin qR_n - qR_n \cos qR_n)^2}{(qR_n)^6}. \tag{8}$$

A volume distribution function is defined as $D(R) = \nu(R)V_p(R)$, where $V_p(R)$ is the volume of the sphere with the radius R.

Equation 7 can be applied also to particles of any shape. Either the size distribution of particles of known shape can be resolved or the particle shape can be resolved if the size distribution is known for example from gel permeation chromatography measurements. The latter case was put into practise in Paper **V** where the ellipsoidal shape of lignosulfonate particles was solved while the former case was used in Papers **II** and **III** to obtain the size distribution of nanoparticles.

The form factor of a scalene ellipsoid with three unequal semiaxes a, b and c cannot be calculated analytically but must be numerically integrated (Pedersen, 1997):

$$P(q, a, b, c) = \frac{2}{\pi} \int_0^{\pi/2} \int_0^{\pi/2} P_{\mathrm{sph}}^2(q, r(a, b, c, \alpha, \beta)) \sin\alpha \, \mathrm{d}\alpha \, \mathrm{d}\beta. \tag{9}$$

Here $r(a, b, c, \alpha, \beta) = [(a^2 \sin^2\beta + b^2 \cos^2\beta) \sin^2\alpha + c^2 \cos^2\alpha]^{1/2}$. If two of the axes are equal, the ellipsoid is called a spheroid. If the axis of symmetry is longer than the two others, the spheroid is prolate (like a cigar), and if it is shorter, the spheroid is oblate (like a pancake).

The object of SAXS studies of colloidal dispersions is typically the determination of the shape of the colloids. In this case dilute dispersions are measured in order to have the structure factor $S(q)$ as close to 1 as possible. In order for the determination of the particle shape to succeed the particles are usually made as monodisperse as possible. Usually the monodispersity or polydispersity of the particles in solution cannot be solved from the scattered intensity. It must be measured with some independent method. Often the particles are assumed to be monodisperse if the Guinier approximation applies in the very beginning of the scattering curve. However, this is not an evidence of monodispersity because it could be caused by only the largest observed particle. In fact, there is no way to know if the sample is monodisperse or not from the scattering intensity unless the scattering is clearly that of some well known particle shape such as a sphere because the form factor of a sphere (Eq. 8) has a very distinct shape. However, a mistake can be made for example if the solution contains monodisperse rods because in this case the scattering intensity looks the same as in the case of a very polydisperse set of spheres.

Electron microscopy techniques would seem to have advantages over scattering techniques because they give the particle size distribution and the shapes of the particles at the

same time. However, in order to get an image, the sample must be prepared in a special manner which essentially modifies the sample. Often one says that x-ray scattering is a non-destructive method and that makes it superior to microscopy techniques. This is not entirely true since the synchrotron radiation commonly used today is so intense that it usually causes radiation damage to biological samples The damage is typically seen either as a burnt spot on the sample or as aggregation in solution samples. The preparation of the samples for electron microscopy, on the other hand, causes artifacts to the sample even before it is measured. The good thing about the scattering methods is that they give a statistical mean of the structure of the sample. Microscopy techniques can probe only a very small part of the sample at a time and that makes them very selective.

Usually SAXS from particles gives one-dimensional data from which a three-dimensional particle is obtained. How is it possible to get a three-dimensional particle from one-dimensional data? Clearly, this demands for assumptions that will affect the resulting particle shape tremendously or we have to know a great deal about the particle before hand by doing other measurements such as electron microscopy, x-ray crystallography or gel permeation chromatography. *You have to make certain assumptions about your sample in order to interpret the result.* This applies in all areas of small-angle scattering and it should be kept in mind when designing an experiment. SAXS can give a confirmation to a theory or reject it. Many structures can cause a similar looking curve and therefore without any understanding of physics or chemistry the results one may obtain can be very speculative.

4.4.2 Scattering from particles with interparticle interactions taken into account

The scattering intensity from an interacting colloidal system typically has a maximum at some q-value which we shall mark q^*. The maximum is called the correlation peak because it originates from the correlations between the colloids. From the position of the correlation peak a Bragg distance $2\pi/q^*$ can be calculated. The Bragg distance is not exactly the average particle spacing but it is a good approximation to it. (Shen *et al.*, 1988)

Some uncertainties regarding the interpretation of the position of the correlation peak need to be understood. The structure factor in Figure 7 has been calculated using the Debye formula for a system of seven particles. The particles were oblate spheroids with axial ratio 5. The scattering intensity is drawn for two particle sizes while the distances between the particles are the same. This means that the structure factor $S(q)$ is the same in both systems (Eq. 3). The position of the correlation peak in the scattering intensity will be different in these two cases because the shape of the form factor $P(q)$ affects the position even if the structure factor $S(q)$ remains the same. This creates uncertainty in the determination of the average particle spacing. When the Porod constant gets smaller the determined average particle spacing will become larger than it truly is. This problem was faced in the analysis of the Porod constant and the average particle spacing in Paper **V**. The two determined parameters were drawn in the same figure (Fig. 9 in Paper **V**) to observe if there is a systematic correlation between them. The changes in the average particle spacing as a function of temperature seem to be caused by real changes in this case because the changes in the position of the correlation peak and in the Porod constant occur at different temperatures. For the concentration series of lignosulfonate, however, it is difficult to say whether the power law observed for the average particle spacing as

a function of concentration is slightly affected by this. In any case, the size of the effect depends on the system.

Even though the position of the peak already tells something about the correlations in the system a more sophisticated analysis is possible if the system is fairly simple. An integral equation that describes the correlations in many body systems was published in 1914 by Leonard S. Ornstein and Frits Zernike. The equation was named the Ornstein-Zernike equation and it can be solved by imposing different closure relations (Hunter, 1992, pp. 703).

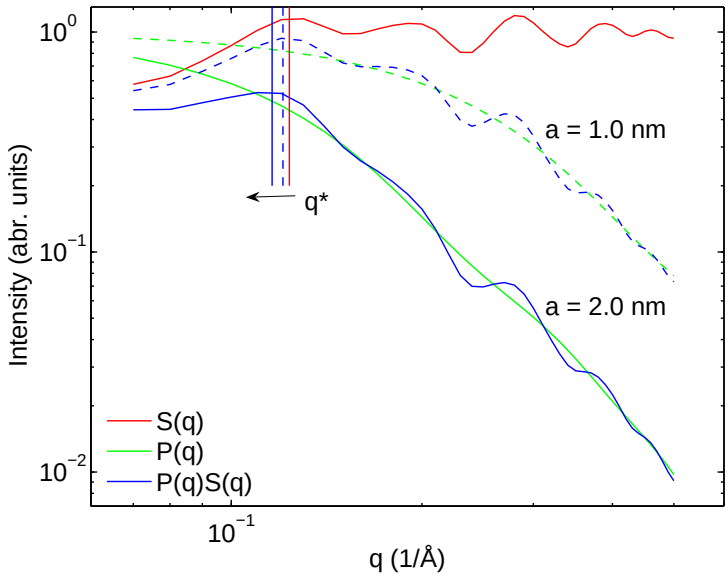


Figure 7: Simulation on how the particle size affects the position of the correlation peak in the scattering intensity curve. Here a is the length of the ellipsoid semiaxis along the symmetry axis. The vertical lines correspond to the determined positions q^* of the correlation peaks. The peak is shifted to smaller values of q when the particle size is increased.

In the study of uncharged polymers which may be approximated as hard spheres it is possible to calculate the structure factor $S(q)$ of such a system by solving the Ornstein-Zernike equation using the Percus-Yevick closure relation (Kinning and Thomas, 1984). The Percus-Yevick structure factor depends only on the distance of closest approach between the hard spheres and on their volume fraction of the total scattering volume. If the structure factor can be solved from the experimental intensity, it will therefore be possible to determine the distance of closest approach between two macromolecules. The limits of the theory are the spherical shape of the particle and the monodispersity although the Ornstein-Zernike equation may also be solved for a polydisperse set of hard spheres (Vrij, 1979).

For charged colloidal systems the Ornstein-Zernike equation can be solved in the mean spherical approximation (MSA) or in the rescaled MSA (Hansen and Hayter, 1982; Hayter and Penfold, 1981). For the charged particles the restriction of the spherical shape is less strict because they do not approach very close to each other due to the electrostatic repulsion. Therefore, this approach can be used for globular particles such as micelles that are not spheres. (Hayter and Penfold, 1983) The solution of the Ornstein-Zernike equation with the mean spherical approximation is semi analytical and complicated, but the solution

has been implemented into at least the small-angle neutron scattering (SANS) package for IGOR Pro (Kline, 2006), which is publicly available (NIST, 2006).

The experimental structure factors of monodisperse systems can be solved from the measured intensities using equation 3 if the form factor of the particle is known (Ottewill *et al.*, 2003). In Paper **V** interacting lignosulfonate macromolecules were studied. However, the effective structure factors could not be correctly computed because the particle size and/or shape changed with concentration. We could therefore present only some very qualitative analysis based on the simple PY model.

4.4.3 Power-law scattering

Many experimental results in physics and chemistry can be analysed by using power laws. The small-angle scattering intensity at least at some q-range typically follows a power law (Schmidt, 1991)

$$I(q) \propto q^{-\alpha}. \tag{10}$$

The power-law exponent α is directly linked to the shape of the particle (see Fig. 6). Sometimes particles and structures can be described by using a fractal model. In the case of fractals one observes power laws with fractional exponents. In real life the statistical fractals are always composed of units of finite size. If the power law is observed between q_{min} and q_{max}, the size of the fractal is about π/q_{min} and the size of the smallest unit in the fractal about $1/q_{max}$. (Schmidt, 1989) See Table 1 for examples of different power-law exponents and the structures they correspond to.

If the power-law region does not extend over many orders of magnitude, the structure cannot necessarily be described with the fractal model. It has been pointed out by Avnir *et al.* (1998) that in almost all publications where the studied system has been claimed to be described by the fractal model the power-law region does not extend over many orders of magnitude. The pitfalls which can cause the fractal interpretation to go wrong are many. For example, polydispersity may cause a power law with a fractional exponent in the scattering intensity (Martin and Hurd, 1987) and the scattering intensity of chain-like polymers in solution will follow a power law that may easily be confused to be arising from platelets (Glatter and Kratky, 1982, chapter 12).

Scattering object	d	D_m	D_s	α	Comment
Thin rod	1			1	
Platelet	2			2	
Mass fractal		D	D	D	$D < 3$
Surface fractal	3	3	D	$6 - D$	$2 < D < 3$
Globular	3	3	2	4	Porod law

Table 1: Some particle shapes that give a $I(q) \propto q^{-\alpha}$ law at the small-angle scattering region. Here d is the Euclidean dimension of the particle, D_m is the mass fractal dimension and D_s is the surface fractal dimension. The globular object may be a sphere or an ellipsoid for example. (Schmidt, 1991)

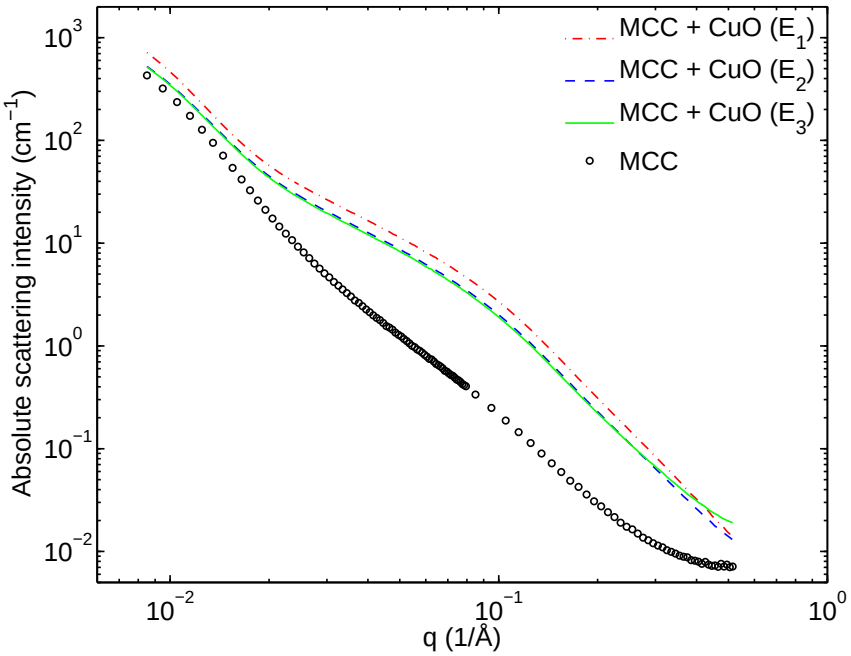


Figure 8: Anomalous scattering intensities of sample 6 near the Cu K-edge (Paper **II**). The sample contained copper oxide nanoparticles and microcrystalline cellulose (MCC). The scattering from pure microcrystalline cellulose is shown for comparison. Only the scattering intensity from copper depends on the energy of the radiation (E_1, E_2 or E_3, see Figure 10 for their values). Notice how the background caused by inelastic processes rises with energy.

4.5 Anomalous small-angle x-ray scattering

Anomalous scattering refers to the situation where the energy of the used radiation is close to an absorption edge of one of the elements present in the studied sample. The scattering factor f changes rapidly near the edge and this makes contrast variation possible. The term resonant x-ray scattering is usually used when experiments are done at the absorption edge.

Although the atomic scattering factor f may usually be approximated in the small-angle x-ray scattering region as the atomic number Z, this approximation is not valid near the absorption edges. Near the edge a complex anomalous dispersion correction term is needed (*e.g.* Als-Nielsen (1993), pp. 20, Elliott (1984), pp. 73)

$$f(q, E) = f_0(q) + f'(q, E) + if''(q, E). \tag{11}$$

Here $f_0(q)$ is the Fourier transform of the electron density of the atom, $f'(q, E)$ is the real part of the dispersion correction, $f''(q, E)$ is the imaginary part and i is the imaginary unit. At small values of q we may approximate $f_0(q) \approx Z$, $f'(q, E) \approx f'(E)$ and $f''(q, E) \approx f''(E)$. The imaginary part of the dispersion correction is related to the absorption of x rays. The change in the scattering factor causes a change in the scattering intensity as seen in Figure 8 for a sample containing copper and microcrystalline cellulose (Paper **II**). See section 4.6 for the details on the determination of the anomalous scattering factors.

Basics of ASAXS have been described in Simon and Lyon (1994) and Haubold *et al.* (1994). After its invention by Stuhrmann in 1981 (Feigin and Svergun, 1987, pp. 140 – 144) the ASAXS technique has not gained as wide user community as for example

the multiwavelength anomalous diffraction (MAD) which is widely used in the studies of structural biology (Hendrickson, 1991). ASAXS has been typically used to study metal alloys and porous catalysts (Goudeau *et al.*, 1986; Goerigk *et al.*, 2003) and recently also to get the distribution of ions around a polyelectrolyte in solution (Dingenouts *et al.*, 2003; Das *et al.*, 2003; Horkay *et al.*, 2006). Whether this is a start of a new era for ASAXS is to be seen in the near future.

In order to describe a system that has many components we need to introduce the so called partial structure factors (PSF) which will be denoted with the symbol $S_{xy}(q)$, where x and y are phases with different electron densities. In a two-component system we have components 1 and 2. To describe such a system we need three PSFs, namely $S_{11}(q)$, $S_{22}(q)$, and $S_{12}(q)$. In a three-component system we have six PSFs and the intensities from systems with even more components become increasingly more difficult to interpret. In practise the two-component model is the most commonly used. The separation between two and three-component systems is not necessarily easy. For example, consider a dilute system with two phases: a macromolecule (phase 1) in a solvent (phase 2). Does it transform into a three-phase system when we add bubbles into the solution? No. The bubbles do not have a scattering factor f (the bubbles are assumed to be nearly vacuum like here) and their contribution vanishes as can be seen in the equation below. However, it does affect the partial structure factors. In the first case the problem can be solved by regular SAXS and ASAXS can only be used to enhance the contrast between the elements. In the second case the PSFs are different from each other because there exists three types of interfaces between the solvent, the macromolecule and the vacuum. For the systems studied in this thesis the two-component analysis was sufficient. Even an alloy of three metals can be analysed as a two-component system (Simon and Lyon, 1994).

For a two-component system consisting of atoms of phase 1 and atoms of phase 2 the x-ray scattering intensity $I(q)$ can then be written as (Ludwig Jr., 1986; Simon and Lyon, 1994)

$$I(q) = x_1|f_1|^2 S_{11}(q) + x_2 f_1 f_2^* S_{12}(q) + x_2 f_1^* f_2 S_{21}(q) + x_2|f_2|^2 S_{22}(q), \tag{12}$$

where $S_{12}(q) = S_{21}(q)$ which causes the imaginary parts to cancel. Here it has been assumed that the atomic fraction x_2 of phase 2 is less than that of phase 1, which causes the coefficient x_2 in front of the cross terms. In the ASAXS analysis the atomic fractions are not necessarily needed because they can be merged into the structure factors without loss of information unless absolute scattering intensities are needed for the PSFs.

Equation 12 can be presented in a matrix form. For example, for intensities from the same sample at three different energies near the absorption edge of phase 2 the equations are

$$\begin{pmatrix} I(q,E_1) \\ I(q,E_2) \\ I(q,E_3) \end{pmatrix} = \begin{pmatrix} \alpha & \beta(E_1) & \gamma(E_1) \\ \alpha & \beta(E_2) & \gamma(E_2) \\ \alpha & \beta(E_3) & \gamma(E_3) \end{pmatrix} \begin{pmatrix} S_{11}(q) \\ S_{12}(q) \\ S_{22}(q) \end{pmatrix}, \tag{13}$$

where $\alpha = x_1 Z_1^2$, $\beta(E) = 2x_2 Z_1[Z_2 + f_2'(E)]$, and $\gamma(E) = x_2[(Z_2 + f_2'(E))^2 + f_2''(E)^2]$. Here it has been assumed that f_1 has only a small anomalous dispersion correction which can be ignored and that f_0 is Z at the small-angle scattering region. For the materials studied in this thesis these are good approximations. In principle the partial structure factors can be solved from the set of equations. In practise the solution is extremely sensitive to errors in the original intensities (Papers **II** and **III**). One way to simulate the effect of the error is to calculate the partial structure factors using the Debye formula so that instead of adding the sum over all points with different atomic scattering factors one simply adds the

contributions from one species with the same f to get the $S_{11}(q)$ and respectively $S_{22}(q)$, and all the contributions where the points have different f to get $S_{12}(q)$. Using such a simulation it was observed that a small error in the f' or in the level of the intensity can cause dramatic effects on the solved PSFs. These effects are due to the sensitivity of the solution to even the smallest errors in the coefficient matrix or in the experimental intensities. Example of such an effect is shown schematically in Figure 9. By measuring the scattering intensities at more than three energies and especially by measuring the intensity from the sample at another absorption edge relevant to the other phase, the problem can be made less ill conditioned. The statistical accuracy of the intensities must be excellent and the energy dependent background needs to be removed in order for the method to be successful.

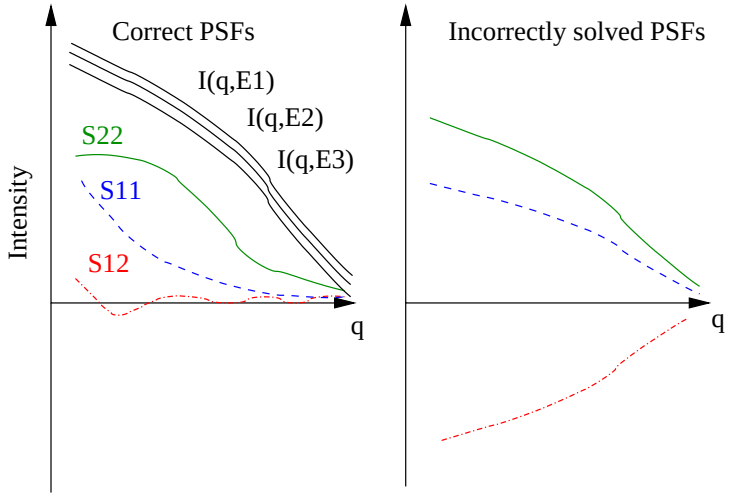


Figure 9: A schematic picture of what the solutions of the PSFs of the two-component system can look like if at one of the energies E_1, E_2 or E_3 the f' has a wrong value when solving the PSFs from the three intensities using equation 13. For example, about 10 % error compared to the correct value of f' could cause this effect. In the incorrect solution all the PSFs have the same shape as the initial intensities from which they were solved and one of them is negative.

Equation 13 can be solved by different means. In Paper **II** we used a derivative method, where the intensities were differentiated with respect to f' in order to get rid of the term that does not change with energy, in this case the PSF of MCC. The $S_{22}(q)$ can then be obtained by fitting a line at each q to $(Z_2 + f_2', \mathrm{d}I/\mathrm{d}f_2')$. The slope of the line is proportional to the $S_{22}(q)$. This method of extracting the PSF is very useful because it allows for the monitoring of the goodness of the data. For example, it is possible to notice if one of the energies is wrongly calibrated. Then one of the points in the graph systematically deviates from the line that fits well to the other points.

Because of the uncertainties in the calculations of the PSFs, differential structure factors (DSF) may be used instead. DSFs are computed by subtracting the intensity obtained at one energy by another intensity obtained at another energy. In this subtraction the PSF that does not change with energy will be subtracted and only the $S_{12}(q)$ and $S_{22}(q)$ terms remain. If the $S_{12}(q)$ can be assumed to be zero this method gives the partial structure factor $S_{22}(q)$.

One of the problems in the data processing of ASAXS is the subtraction of an energy

dependent background from the data. Below the absorption edge, resonant Raman scattering becomes more and more dominant. It gives a constant background which cannot be eliminated by using a 2D detector with a poor energy resolution. Fluorescence gives also a constant background and especially above the edge the contribution from fluorescence is high. (Wilson, 1995, pp. 570 – 578) The energy dependent background can be subtracted for example by fitting a power law and a constant to the tail of the scattering curve and by subtracting the constant. This is how it was done in Papers **II** and **III**.

Another way to deal with systems that require contrast variation is to measure small-angle neutron scattering where different isotopes of the same elements have different scattering factors. One can also introduce a different scattering contrast to one of the phases and do regular SAXS. In the case of cellulose embedded nanoparticles the scattering from pores may be suppressed by filling them with some liquid that has electron density close to that of cellulose. In such a way the metallic nanoparticles are the only source of contrast. With this approach only the incoherently scattered background needs to be subtracted. Water could act as a contrast remover of cellulose in the cellulose metal nanoparticle systems. This is presently being tested in the laboratory by K. Pirkkalainen. Since the nanoparticles studied in Papers **II** and **III** were made in aqueous solution, the adding of water to the samples should not present any dramatic chemical changes in the nanoparticles.

4.6 X-ray absorption

Even though the absorption of x rays by gas is a relatively simple phenomenon, the absorption of x rays by condensed matter is very complex. The structure of the absorption curve near the edge is called x-ray absorption near edge structure (XANES) or near-edge x-ray absorption fine structure (NEXAFS) and the oscillations far from the edge above the threshold energy go by the name extended x-ray absorption fine structure (EXAFS). The first observations of the complicated structures of the absorption edges were done in the beginning of 1920s while the first theories explaining the EXAFS structure were published in the beginning of 1930s. The Fourier transform analysis of EXAFS, however, was not adopted until the beginning of 1970s. (Lyttle, 1999)

Ab initio theories explaining the absorption of x rays by bound electrons are being improved constantly and currently they can already explain the fine structure of the absorption edge both near and far from the edge (Rehr, 2006). The near-edge structure gives information on the bonding of atoms. By XANES measurements metallic and oxidised metals can be distinguished. In Paper **II** for example the crystalline phases in the samples containing the least amount of copper were difficult to identify using XRD because the signal from the copper compared to the cellulose was so weak. From XANES, however, it was clearly seen that the copper was in oxidised state. In fact, in the case of mixed phases XANES data can be used to evaluate the amount of each phase by comparing the XANES curve of the sample to those of standards. In Papers **II** and **III** XANES data was used to determine accurately the amount of metal in the samples and qualitatively the chemical state of the metal atoms.

Chantler *et al.* (2005) give an extensive tabulation of the theoretical absorption coefficients of non-interacting atoms. Figure 10 illustrates the differences between the experimental and the theoretical anomalous scattering factors of free Cu atoms. Due to the fine structure of the absorption edge, the theoretical values of the anomalous dispersion corrections may not be good enough for the purposes of ASAXS. Furthermore, the determination

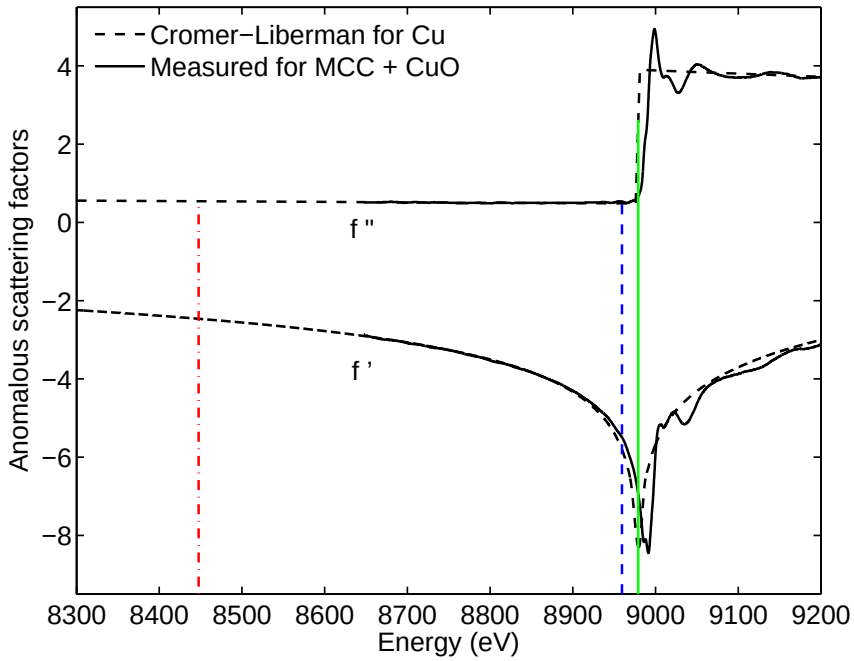


Figure 10: Anomalous scattering factors f' and f'' of the same sample as in Figure 8 and theoretical ones (Merritt, 2003). The energies used in the ASAXS experiment are indicated by vertical lines.

of the absolute position of the energy scale is not trivial. Therefore the absorption curves extending to the EXAFS region were used to determine the anomalous scattering factors of the metal atoms in Papers **II** and **III**. The imaginary part f'' is directly related to the absorption and the real part f' is obtained through the Kramers-Kronig relation for example by using the program CHOOCH (Evans and Pettifer, 2001). In an ASAXS experiment a rather large energy region needs to be accessible to be able to have sufficiently large variation in f' without any change in the position of the beam on the sample. Not only must the region be wide but it needs to be covered with an excellent energy resolution.

5 Results and discussion

5.1 Cellulose-based materials

In the study of cellulose-based materials the first step is to identify the structure of the cellulose in the samples. The scattering intensities of cellulose Iα and Iβ were calculated from atomic coordinates obtained from Nishiyama *et al.* (2003) and Nishiyama *et al.* (2002) by using the *Mercury* software (Bruno *et al.*, 2002). The calculated intensities are presented in Figure 11 together with experimental intensities from cellulose- and lignin-based materials. The full width at half maximum (FWHM) of the reflections in the calculated intensities were set to 1.5 degrees for comparison.

The microcrystalline cellulose in the samples containing copper and nickel (Papers **II** and **III**) is more precisely described by the cellulose Iβ-allomorph than the Iα-allomorph according to Figure 11. For the cellulose in Sitka spruce it is impossible to say from the diffraction pattern whether it is cellulose Iα or Iβ. It is generally accepted though that

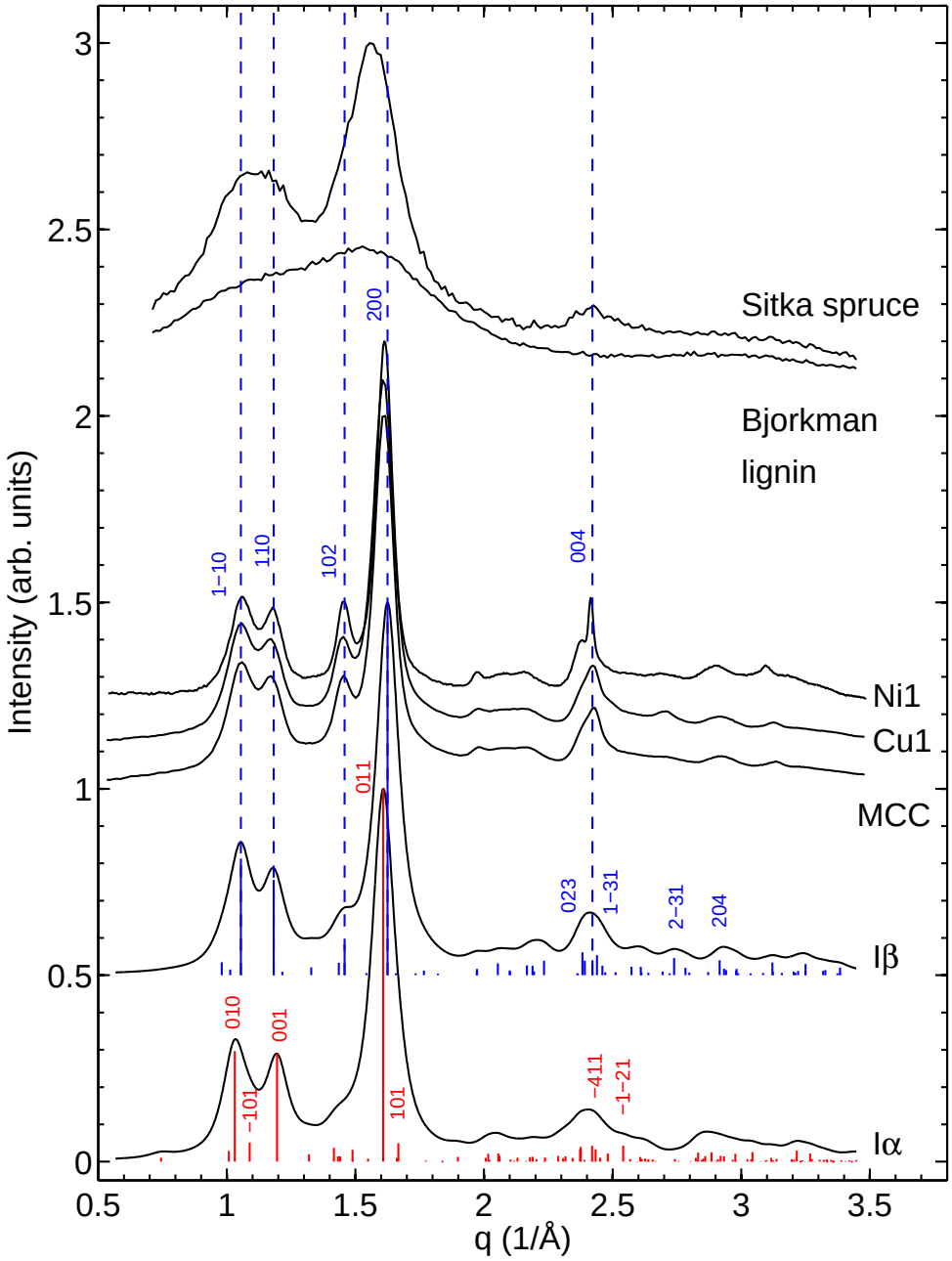


Figure 11: Calculated scattering intensities of cellulose Iα and Iβ-allomorphs, theoretical positions of the reflections with the most intensive reflections marked with Miller indexes, and measured scattering intensities from microcrystalline cellulose from cotton (MCC, Paper **II**) and copper (Cu1, Paper **II**) and nickel (Ni1, Paper **III**) supported on MCC, Björkman lignin and Sitka spruce sample from Washington provenance (Paper **I**). The curves are moved vertically for clarity.

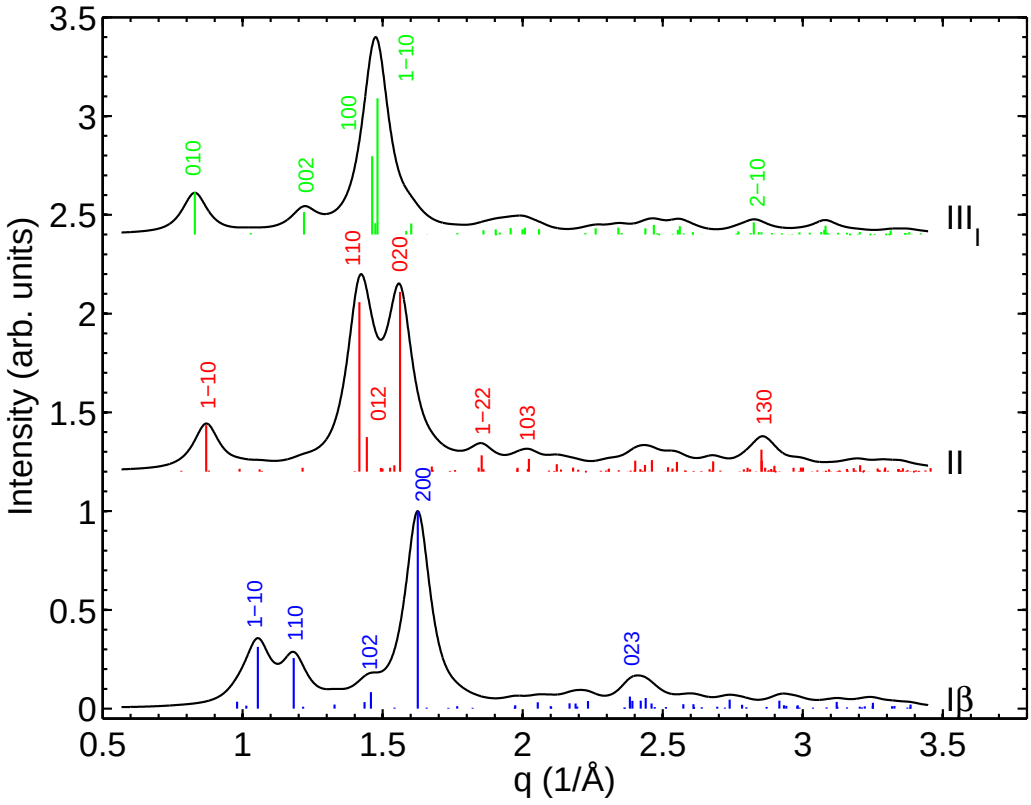


Figure 12: Calculated scattering intensities of cellulose II (Langan *et al.*, 2005) and III_I (Wada *et al.*, 2004a) compared to that of cellulose Iβ.

higher plants like wood mostly contain cellulose Iβ. With this in mind we assume all of the cellulose presented in this thesis to contain mostly cellulose Iβ and therefore the reflections in the diffraction patterns are indexed as in Iβ. The crystallite size in the direction normal to the plane (200) was calculated for the Sitka spruce samples to be about 3.0 nm using the Scherrer formula (Paper **I**) while for the microcrystalline cellulose obtained from cotton by mild acid hydrolysis the crystallite size in the same direction was about 7.3 nm (Papers **II** and **III**). For all the measured samples the reflection 200 is shifted to smaller angles compared to the theoretical position. This could be explained by lattice expansion. For smaller crystallites of Sitka spruce the expansion is more pronounced than for the larger crystallites of MCC. This sort of lattice expansion or contraction in nanometre sized crystallites is also typical for inorganic compounds. The expansion in only the direction perpendicular to the plane (200) is explained by the fact that the cellulose chains are kept together in the direction normal to plane (200) only through weak electrostatic bonds and van der Waals interaction. In the direction normal to plane (004), where the forces are covalent along the chain, lattice expansion is not observed or the effect is very small as expected for large crystallites.

5.1.1 Coordination of metal ions onto cellulose

The chemical reduction of transition metal ions within a cellulose support might have some effect on the crystalline structure of cellulose. From the scattering intensities of the samples this seems not to be the case because the scattering intensities of pure MCC and

the samples containing nickel and copper are practically the same as is shown in Figure 11 except for the contributions from the metal compounds. The calculated scattering intensities of the modified celluloses are very different from the Iβ-allomorph (see Figure 12), so we may safely say that the structure of cellulose is not changed in the chemical process.

When transition metal ions were reduced in the solid cellulose support in aqueous solutions, a size distribution of nanoparticles containing the metal was observed (Papers **II** and **III**). The size distributions of the nanoparticles were studied using anomalous small-angle x-ray scattering and the crystallinity by wide-angle x-ray scattering. It was observed that the size distribution of copper oxide nanoparticles correlated with the sizes of the copper oxide crystallites. The nickel containing nanoparticles were amorphous, so a similar comparison with the crystallite sizes could not be done. When the reduction of nickel ions was done in water, there were only large nanoparticles. When the reduction was done in ammonium hydrate medium, the samples contained a large amount of very small metal nanoparticles in addition to larger ones. Nickel and copper are known to form coordination complexes with ammonium and this may be the key into the understanding of the formation of the small nanoparticles.

Cupric hydroxide in aqueous ammonia is known to dissolve cellulose. It breaks some of the hydrogen bonds in native cellulose and the copper ions bind coordinatively to the deprotonated hydroxyl groups of cellulose. (Saalwächter *et al.*, 2000) Even though the crystalline structure and crystallinity of cellulose is not changed (to a notable degree) in the chemical processes in Papers **II** and **III**, the possibility that the copper-ammine or nickel-ammine complexes would diffuse into the cellulose matrix cannot be completely excluded. The cellulose fibres are very porous, so another explanation is that some of the ions are stuck in very small pores which would restrict their growth. The nanoreactor model proposed by He *et al.* (2003) would explain the different particle sizes if without the ammonium, the metal ions do not form a coordination complex with the cellulose as easily. This is supported by the finding in Paper **II** that the less ammonium was used the less of the copper was retained in the samples after the reduction and washing.

5.1.2 Thermal expansion of cellulose

Microcrystalline cellulose is of significant importance to the pharmaceutical industries. The good dispersion of drug molecules is necessary. Despite the name *microcrystalline* cellulose (MCC), the crystallinities of commercial microcrystalline celluloses have been determined to be typically about 60 – 70 % and the amorphous content can be increased by ball milling (Suzuki and Nakagami (1999) and references therein). In addition, cellulose fibres are used in the textile industry in natural (e.g. cotton) and regenerated forms. The regenerated fibre materials are called viscose in Europe and rayon in USA. In this respect, such properties of cellulose as the glass transition and the coefficient of thermal expansion have been studied surprisingly little until recently.

The thermal expansion of cellulose in wood has been studied recently by Hori and Wada (2005) and the thermal decomposition of cellulose by Kim *et al.* (2001). Thermal expansion of the lattice parameter a of the cellulose Iβ unit cell is shown in Figure 13. The data was obtained from the scattering intensities of the composites consisting of nickel nanoparticles and microcrystalline cellulose (Paper **III**). The thermal expansion coefficient α of the lattice parameter a was calculated from reflection 200 and by using the same definition as Hori and Wada (2005) and Müller *et al.* (2006)

$$\alpha = \frac{\mathrm{d}a}{\mathrm{d}T}/a(T = 0\ ^\circ\mathrm{C}). \quad (14)$$

At ambient temperature the lattice parameter a is 0.7784 ± 0.0008 nm (Nishiyama *et al.*, 2002), which is close to the value obtained here: 0.781 ± 0.005 nm. The lattice parameter as well as many other properties of crystalline materials are known to depend on the crystallite size (Ayyub *et al.*, 1995), but in our study the absolute error of the q-scale calibration is too large to allow for any solid conclusions.

A transition region in the thermal expansion, typical for materials with a glass transition temperature, is observed at about 170 °C. Due to the uncertainty of the temperature inside the sample, the real temperature of the transition can deviate from the observed one even as much as 10 °C. Hori and Wada (2005) observed that in tension wood sample of poplar (*Populus maximowiczii* A. Henry) the transition temperature was 180 °C, while for a same kind of wood sample the transition was observed previously to be around 200 °C from less precise measurements (Kim *et al.*, 2001).

The temperature scale could have been calibrated accurately by dispersing for example annealed gold crystals to the sample so that the well known thermal expansion coefficient of gold could have been used to get the accurate temperature inside the sample (Seitsonen and Mikkonen, 1973). However, such calibration was not used in the measurements. The relative error of the temperature within the sample based on the degradation temperature of cellulose, between 300 and 350 °C (Kim *et al.*, 2001), is about 5 %. The crystallisation of the nickel compounds within the MCC matrix occurs on the same relative temperature scale and we can observe if there is a correlation between the crystallisation of the nickel compounds and the thermal expansion or degradation of the MCC matrix.

Hori and Wada (2005) reported a coefficient of thermal expansion $\alpha = 13.6 \cdot 10^{-5}$ 1/K for the lattice parameter a before the transition temperature while we observe $\alpha = 9.3 \cdot 10^{-5}$ 1/K. In a more recent study of poplar tension wood $\alpha = (9.9 \pm 0.4) \cdot 10^{-5}$ 1/K for a was obtained from measurements in the temperature range from -73 to 22 °C (Müller *et al.*, 2006). Seitsonen and Mikkonen (1973) studied the thermal expansion of cotton cellulose and their results coincide very well with the values observed here for the microcrystalline cellulose, which is prepared from cotton using mild acid hydrolysis. In that study they did not report an exact transition temperature but showed that the change is continuous and occurs around 150 and 200 °C. Similar results on cotton have also been published by Takahashi and Takenaka (1982). None of these publications give an explanation for the transition. The comparably weak C−H$\cdots$O bonds and van der Waals interactions in the direction normal to plane (200) compared to the strong hydrogen bonds and covalent bonds in other directions do not explain the more rapid expansion in the direction perpendicular to the hydrogen bonded sheets. This is because cellulose II and cellulose $\mathrm{III_{II}}$, which both have hydrogen bonds also between sheets, show a similar expansion in the direction perpendicular to the glucose rings (Hori and Wada, 2006).

The glass transition of dry microcrystalline cellulose has been determined by using modulated temperature differential scanning calorimetry to be a three step process with steps at 132, 159, and 184 °C (Picker and Hoag, 2002). The transition temperatures did not depend on the source of cellulose (softwood or hardwood). The strongest transition was at 159 °C, the next strongest transition at 184 °C, while transition at 132 °C was very weak. This data was just recently correlated to the changes in the strength of intrachain hydrogen bonding by Watanabe *et al.* (2006). Indeed, the transition temperatures could be correlated with changes in the Iβ inter- or intrachain bonding and more accurately to

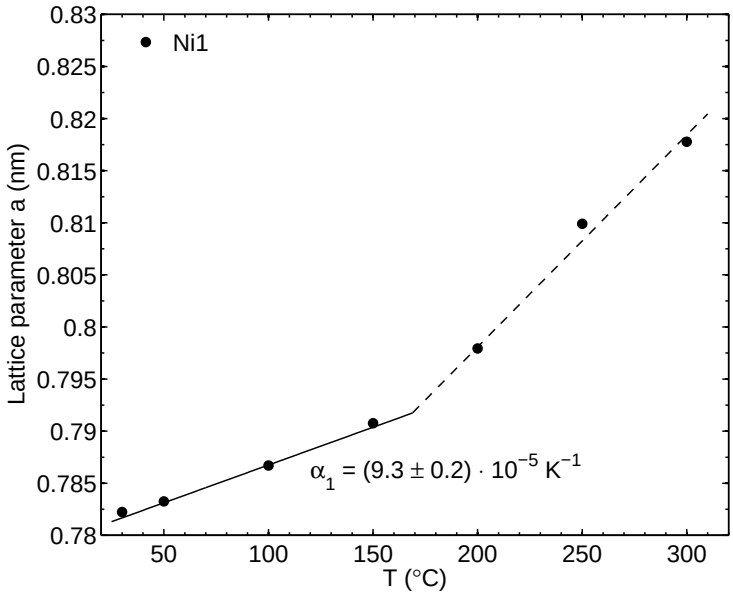


Figure 13: The thermal expansion of the lattice parameter a of the cellulose Iβ unit cell in one of the nickel containing samples (Paper **III**). The dots are the experimental points obtained for sample 1 and the lines are fits to the experimental points obtained for all the samples. The thermal expansion coefficient α relative to $T = 0$ °C and the statistical 1σ error limits are shown. The figure is in the same scale as in Hori and Wada (2005) for comparison.

	Crystalline phase				
Sample	*m.*	fcc Ni	hcp Ni	Ni_3P	NiO
Ni1	-	300 °C	300 °C	-	350 °C
Ni2	250 °C	400 °C	-	250 °C	-
Ni3	-	300 − 350 °C	-	300 − 350 °C	-
Ni4	300 − 350 °C	400 °C	-	350 °C	-

Table 2: The crystalline phases of Ni nanoparticles supported on microcrystalline cellulose were identified from the diffraction patterns upon heating. Symbol *m.* refers to metastable phases composed of Ni and P. The details of the synthesis of the samples are explained in Paper **III**.

intrachain bonding O3−H3···O5. If the intrachain bonding is weakened, one would expect the cellulose chains to lose their stiffness.

Apparently, the transition in the thermal expansion of the microcrystalline cellulose crystallites is not connected to the crystallisation of the amorphous nickel nanoparticles. The temperatures at which for each sample the reflections arising from the crystalline nickel compounds were observed for the first time upon heating are listed in Table 2. For sample 2 the first measurement above 50 °C was done at 250 °C and thus the crystallisation might have begun at even lower temperatures. (Paper **III**)

The degradation of cellulose occurs between 300 and 350 °C. The crystallisation of nickel compounds in the samples begins just before the cellulose is fully degraded. However, there is at least one other factor that determines the crystallisation temperature of nanoparticles

and that is their size. The size distribution of the nanoparticles could be determined using ASAXS assuming a spherical particle shape and no inter-particle correlations. According to Paper **III** in samples 3 and 4 made in ammonium hydrate solution there is a much larger fraction of particles with size less than about 20 nm than in samples 1 and 2 made in aqueous solution. In sample 3 the number of these small particles is far greater than in any of the other samples. Against expectations, the samples in which smaller particles are observed start to crystallise at higher temperatures than the samples where there are larger particles. The question whether the cellulose matrix affects the temperature where the crystallisation starts cannot be answered by these measurements. However, the thermal expansion coefficient and the degradation temperature of cellulose did not vary from sample to sample (including pure MCC), which means that at least the cellulose is not affected by the crystallisation of the nanoparticles.

5.1.3 Cellulose in wood

In Paper **I** the mean microfibril angle in Sitka spruce near the pith was observed to be high and it was shown that as a function of the annual ring the MFA decreased in a fashion characteristic to each provenance. Recently the MFA of Norway spruce and Scots pine grown in Northern Europe have been characterised in detail with x-ray diffraction (Sarén, 2006; Andersson, 2007). The MFA distributions in single cell walls of Norway spruce fibres could be measured using a very narrow synchrotron radiation beam that was directed through a bordered pit in the fibre (Peura *et al.*, 2005). The results obtained for the MFA in Paper **I** were obtained for samples with a thickness of about 1 mm. For such samples the distribution will also be affected by the different orientations of single wood fibres in the sample. However, the method has proved to be successful in determining the mean MFA.

In the case of Sitka spruce there were significant differences in the MFA between trees grown from seeds that were collected from different provenances. The mean MFA near the pith was observed to remain large even at about 10 to 14 rings from the pith. The thickness of the cellulose crystallites in the direction perpendicular to the crystallographic plane (200) was observed to be about 3.0 nm which is smaller than that observed previously for Norway spruce (Andersson *et al.*, 2003) and for Sitka spruce (Hori *et al.*, 2002). The thickness of the cellulose crystallites can differ even within one species and it is known that the thickness does not systematically depend on the MFA (Andersson *et al.*, 2003).

Previously the MFA of Sitka spruce has been studied as a function of the year ring by Philips (1941). He reported that the MFA of Sitka spruce decreases very rapidly from a large value near the pith to a small stable value at about six to nine rings from the pith. This is in contradiction to the results that were obtained in Paper **I**. Cowdrey and Preston (1966) measured the helical angle in two disks of Sitka spruce as a function of the annual ring and obtained for one of the disks a similar trend as we observed for the trees from Washington and Oregon provenances. Hori *et al.* (2002) determined the MFA of three samples of Sitka spruce, but they did not specify the annual rings studied nor the growth conditions or the origin of the trees from which the samples were taken. They found the MFA of their samples to be rather small (6 – 12°) and the width of the cellulose crystallites to be about 3.4 – 3.8 nm.

The heritability of MFA in *Pinus radiata* has been studied with clones using a polarised light microscopy technique. Significant variations were found among the clones, but also within and between trees for each clone. (Donaldson and Burdon, 1995) It is a ques-

tion whether the large differences between the Sitka spruce trees originally from different provenances can be evened by silviculture.

5.2 Lignin-based materials

Langmuir-Blodgett (LB) films of lignins have been studied with microscopy techniques, and based on those studies lignins are considered to be flat particles (Pasquini *et al.*, 2002). Nevertheless, due to the polydisperse nature and other interesting phenomena that occur in aqueous solutions of lignins, there exists confusion whether the molecules after all are spherical in solution due to the amazing amount of different results (Paper **IV**). Observing of soft branched polymers on a surface does not necessarily reveal what is the shape of the particles in solution. For example dendrimers that have a globular shape in solution may deform on a surface to a flat shape (Mecke *et al.*, 2004)

Pasquini *et al.* (2002) studied LB films of ethanol lignin and saccharification lignin with atomic force microscopy and infrared spectroscopy. They found ellipsoidal aggregates perpendicular and parallel to the surface. They did not specify any dimensions for those ellipsoids nor whether they were oblate or prolate. In Paper **IV** we demonstrated with SAXS measurements from kraft lignin solutions that on the average an elongated flat shape described the kraft lignin particles in saline and NaOH solutions. In this study the polydispersity of kraft lignin was 2.1, in which case the polydispersity already starts to affect the particle shape determination. However, the lignin particles are not all of the same shape so the obtained shape may be regarded as a sort of an average shape. In Paper **V** an attempt was made to take the polydispersity into account by using the gel permeation chromatography data to get the number size distribution of the particles and by fitting the shape of the particle. Oblate spheroids with an axial ratio of about 3.5 were found to describe well the shape of the lignosulfonate particles.

The shape of the lignin particles is of interest both because it plays an important role in the cell walls but also from applications point of view. Composite films have been made from lignosulfonate–starch (Baumberger *et al.*, 1997) and kraft lignin–starch (Baumberger *et al.*, 1998) blends with lignin content up to 30%. The strength of the lignosulfonate–starch films was higher and the elongation was smaller than that of pure starch. The kraft lignin–starch films were inhomogeneous and in different humidities the strength of the films either increased or decreased as a function of lignin content. Whether these composite materials and their related applications will become popular remains to be seen. Lignin derivatives are usually brown and that can cause some limitations.

In Paper **V** the association of lignosulfonate particles was observed as a function of lignosulfonate concentration. During industrial processes the dispersion of lignin into the mass of other polymers is affected by the association tendency of the lignin macromolecules. The strength of lignin–polymer complexes is determined by the physical and chemical interactions of the lignin macromolecules with the other polymers.

Lignosulfonates were observed in Paper **V** to associate fairly minimally even at high temperatures and concentrations of lignosulfonate. Kraft lignin which is less soluble in water is more prone to association. Figure 14 shows the distance distribution functions (see Equation 6) of kraft lignin and lignosulfonate (Papers **IV** and **V**). The conditions of the solutions were nearly similar but the molar masses of the fractions are different. However, the maximum size of the molecules is about the same and this indicates much stronger association of the kraft lignin particles.

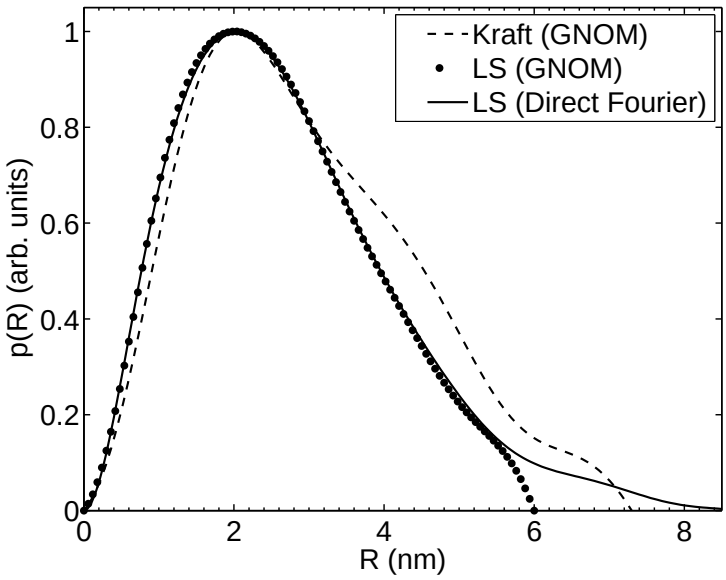


Figure 14: Distance distribution functions $p(R)$ of 5 g/l kraft lignin (*Kraft*, M_w = 5800 g/mol, Paper **IV**) in 0.1 M NaCl aqueous solution and of an infinitely dilute solution of lignosulfonate (*LS*, M_w = 18 000 g/mol, Paper **V**) in 0.2 M NaCl aqueous solution. R is the distance between two points in the particle. Both lignins have polydispersity 2.1. The distributions were calculated either by a direct Fourier transform or by indirecct Fourier transform using the program GNOM.

Figure 14 shows also another interesting feature. Because these lignin dispersions are polydisperse, the distance distribution function $p(R)$ does not correspond to the $p(R)$-function of a single particle but it is an average over many particle sizes. This means that the maximum size given by the largest R for which the distribution is non-zero corresponds to the largest dimension of the largest particles. However, for lignosulfonate the figure shows two distributions which were obtained by different methods. One was determined by direct Fourier transform of the scattering intensity (Eq. 6). The GNOM program package (Svergun, 1991), however, solves the $p(R)$-function by indirect Fourier transform and regularisation. The maximum diameter is given to the program as an input parameter, but by testing several diameters it is possible to find which diameter gives the best fit and to use that one. The difference in the maximum diameter between the indirect and direct results represents the uncertainty of this determination, but also other factors may affect the results of the GNOM program which assumes that the scattering is from a monodisperse particle.

Because of the strong self-association of the kraft lignin particles, the shape of the associated kraft lignin macromolecules may be different from that of lignosulfonate macromolecules. It is also clear that the association may affect the shape of the molar mass distribution in different solvents because the distribution is typically determined under conditions where association is avoided. A simple shifting of the distribution to larger molar masses like done in Paper **V** may not be enough to correct for the difference. However, because it is not possible to fit both the shape of the distribution and the shape of the particle, one always needs to assume either a shape for the distribution or a shape for the particle. Therefore, the use of the approximately log-normal shape of the size distribution

determined by gel permeation chromatography is justified.

Radius of gyration of the particles could be determined by using the Guinier approximation. The radius of gyration is also a measure of the association because associated particle complexes will have a larger radius of gyration. It is interesting to note how differently kraft lignin and lignosulfonate behave in saline solutions. The radius of gyration of kraft lignin was observed to be larger in 0.025 M NaCl solution than in 0.1 M NaCl solution. An opposite phenomenon is observed for lignosulfonate in which case the salt contributes to the association. As a function of the increasing concentration of lignin the association of kraft lignin in 0.1 M NaCl is observed to be much more stronger than the association of lignosulfonate in water or in 0.2 M NaCl solution. These differences are mostly due to the differences in the chemical structure of the lignin derivatives. However, based on just these two studies it is not possible to say whether the molar mass of the fraction plays a role in the association behaviour.

The association and the aggregation of kraft lignin has been studied extensively by viscosity (Lindström, 1979), turbidity and quasi-elastic light scattering measurements (Norgren *et al.*, 2001, 2002). It is inevitable that the association will be somehow connected to the final structure of the aggregates and that the structure of the aggregates will tell about the association.

One of the indicators of the compactness of the aggregate or a macromolecule is the density. The density of the aggregate depends on how tightly the macromolecules can be packed. In the studies carried out in Papers **IV** and **V** the density of lignin macromolecule was assumed to be 1.4 g/cm^3. The value of the density is crucial in the determination of the volume fraction and the electron density of lignin. The value was taken from the publication by Stamm and Hansen (1937). Nearly the same fairly high density, 1.35 g/cm^3, was used for lignin in a study where a fractal model was used in the interpretation of the morphology of modelled lignin (Jurasek, 1996).

Several studies have tried to explain the hydrodynamic properties of lignins by using the concept of fractals (Karmanov and Monakov, 1996). The fractal model has been tested with other methods such as light scattering (Merkle *et al.*, 1992; Norgren *et al.*, 2002) and by microscopy techniques (Radotić *et al.*, 2000, 2005). A fractal ordering of the macromolecules has been observed both in solution and in the solid state for different types of lignins.

In Paper **IV** it was shown that the fractal idea does not apply to the released suspension culture lignin which is considered to be in more natural state than the lignins separated chemically or mechanically from the cell walls. For kraft lignin the fractal approach was successful, but the other studied lignins had compact structures. In another study the SAXS intensities of several lignins were measured while heating the lignins in a nitrogen atmosphere (Vainio *et al.*, 2002). The scattering intensity of lignosulfonic acid had two short power-law regions with exponents -3.3 and -1.5, but these exponents were observed to be different in different samples of lignosulfonic acid. In addition, the scattering intensity of lignosulfonic acid was observed to increase with temperature on the contrary to other lignins. The SAXS intensity of kraft lignin remained constant up to 220 °C where a slight decrease in the intensity was observed. This indicates that the softening temperature of kraft lignin is very high in the dry state. The intensity of milled wood lignin decreased dramatically above 180 °C, while the intensity was observed to decrease above 160 °C in the case of steam explosion lignin and already above 80 °C in the case of Alcell organosolv lignin. This shows how dramatic changes the different separation methods can have on the

chemical and physical properties of lignins. The decrease in the intensity may be assigned either to softening of the lignin derivatives at glass transition or even to degradation.

Goring (1963) has determined the softening temperatures of several lignin derivatives in dry and moist states by using a system where the sample powder was compressed under a constant load in a glass capillary. It was shown that the moisture content and the molar mass of the lignin fraction as well as the separation method played a crucial role. The highest softening temperature was found for softwood sodium lignosulfonate at 235 °C in the dry state, and when the mass fraction of water in the sample was 0.17 the softening temperature was also one of the highest for lignins, namely 118 °C. The lowest softening temperature was found for aspen dioxane lignin for which the softening temperature was 134 °C in the dry state and 78 °C in the moisturised state. The softening temperature depended also on the molecular mass of the lignin macromolecules in such a way that the lignins with smaller molecular mass had a lower softening temperature.

The softening might be of meaning when we study the morphology of solutions with different concentrations of lignosulfonate or kraft lignin. Goring (1963) studied the effect of water content on the softening temperature of periodate lignin and found that the softening temperature decreased with increasing moisture content, reaching a plateau at about 30 % water content. The softening temperature of periodate lignin from spruce at that moisture content was about 90 °C. Because the softening temperatures of lignins in the moist state were fairly high, there is reason to believe that also in more dilute solutions the molecules will be in the glassy state in room temperature. In Paper **V** the lignosulfonate solutions were heated up to 50 °C and this temperature is still smaller than the softening temperatures reported above. This would support the interpretation that the decrease in the surface-to-volume ratio is caused by association of the stiff oblate particles rather than changes in the conformations of the molecules in the particles.

In the study of Goring (1963) the thermal softening of cellulose was not observed before the degradation of cellulose. This means that he did not observe the transition at about 170 °C that was observed by x-ray diffraction (see section 5.1.2). It is questionable whether the softening temperatures of lignins are then correctly determined. However, as he stated in his study, thermal degradation was not usually observed in the case of the lignins at the softening temperature and therefore the temperatures reported for lignins should be reliable. In addition, Irvine (1984) has reported the glass transition of water saturated milled wood lignins to be 45 – 75 °C depending on the origin of the lignin.

6 Future aspects

The demand for sustainable materials and sustainable development continues to grow. Even though the sustainability of lignin has been questioned (Scott and Wiles, 2001), it is believed that in the future the pulp mills will be modified into biorefineries producing not only pulp and energy but also a variety of chemical feedstocks for biomaterials. In this scenario kraft lignin would serve as a resource for new polymers, composites and fuels. (Chakar and Ragauskas, 2004)

It has been shown in this thesis that the interactions of lignin macromolecules in aqueous solvents are of interest by themselves as there exists both attractive and repulsive forces between the lignin particles. Because the morphology of the lignin particles obtained from a pulping process vary from one particle to another, lignin probably will not serve as a perfect model compound for studies of these sort of interactions even though the average shape

of the particles is known. Nevertheless, lignosulfonate has been considered as a kind of a model compound to mimic proteins (Mafé *et al.*, 1995). Unlike proteins lignin is branched and therefore it cannot "unfold" like proteins under any conditions. Furthermore, from the industrial side the benefits of understanding the interactions of lignin include better understanding of the reasons why problems may occur in the processes in certain conditions.

In the future it may be interesting to study the distribution of counterions around the lignosulfonate macromolecules by anomalous small-angle x-ray scattering. Studies as a function of temperature would be particularly interesting because the association of the counterions onto the macromolecule could be studied in more detail. Also the behaviour of the lignosulfonate solutions at the high concentrations might be understood better.

Cellulose has been studied for long and the challenges are in using the cellulose as a starting material for new materials. Recently it was noticed that ionic liquids can be used to dissolve cellulose (Zhu *et al.*, 2006). This will open up new interesting ways to use cellulose. X-ray scattering methods will once again play a key role in the characterisation of those materials.

The characterisation of the structure of Sitka spruce revealed interesting trends in the mean microfibril angle as a function of the annual ring. These trends were different in the trees whose seeds were imported from different locations from North America. The heritability of MFA and the effect of silviculture on the mean MFA of Sitka spruce should be studied in more detail because the MFA was so strongly affected by the location of the provenance. This would require controlled sample conditions and a large amount of samples in order to be able to make biologically relevant conclusions. The project would last at least a few decades, perhaps an unrealistic duration for a scientific project in todays world.

References

Adler E. *Ligninets kemiska bygnad.* Svensk kemisk tidskrift **80(9)** (1968), 279 – 290. In Swedish.

Aimi H, Matsumoto Y and Meshitsuka G. *Structure of small lignin fragments retained in water-soluble polysaccharide extracted from sugi MWL isolation residue.* J. Wood Sci. **50** (2004), 415 – 421.

Åkerholm M and Salmén L. *The oriented structure of lignin and its viscoelastic properties studied by static and dynamic FT-IR spectroscopy.* Holzforschung **57** (2003), 459 – 465.

Als-Nielsen J. *Diffraction, refraction and absorption of x-rays and neutrons: A comparative exposition.* In *Neutron and synchrotron radiation for condensed matter studies*, vol. I. Theory, instruments and methods. EDP Sciences - Springer-Verlag (1993).

Andersson S. *A study of the nanostructure of the cell wall of the tracheids of conifer xylem by x-ray scattering.* Ph.D. thesis, University of Helsinki (2007). http://ethesis.helsinki.fi/en/.

Andersson S, Serimaa R, Paakkari T, Saranpää P and Pesonen E. *Crystallinity of wood and the size of cellulose crystallites in Norway spruce (Picea abies).* J. Wood Sci. **49** (2003), 531 – 537.

Atalla RH and VanderHart DL. *Native cellulose — A composite of 2 distinct crystalline forms.* Science **223(4633)** (1984), 283 – 285.

Avnir D, Biham O, Lidar D and Malcai O. *Is the geometry of nature fractal?* Science **279(5347)** (1998), 39 – 40.

Ayyub P, Palkar VR, Chattopadhyay S and Multani M. *Effect of crystal size reduction on lattice symmetry and cooperative properties.* Phys. Rev. B **51(9)** (1995), 6135 – 6138.

Azároff LV, Kaplow R, Kato N, Weiss RJ, Wilson AJC and Young RA. *X-ray Diffraction.* McGraw-Hill Book Company (1974).

Baumberger S, Lapierre C, Monties B and Della Valle G. *Use of kraft lignin as a filler for starch films.* Polym. Degrad. Stab. **59** (1998), 273 – 277.

Baumberger S, Lapierre C, Monties B, Lourdin D and Colonna P. *Preparation and properties of thermally moulded and cast lignosulphonates-starch blends.* Ind. Crop. Prod **6** (1997), 253 – 258.

Bruno IJ, Cole JC, Edgington PR, Kessler M, Macrae CF, McCabe P, Pearson J and Taylor R. *New software for searching the Cambridge Structural Database and visualizing crystal structures.* Acta Crystallogr., Sect. B: Struct. Sci **58** (2002), 389 – 397.

Chakar FS and Ragauskas AJ. *Review of current and future softwood kraft lignin process chemistry.* Ind. Corp. Prod. **20** (2004), 131 – 141.

Chantler CT, Olsen K, Dragoset RA, Kishore AR, Kotochigova SA and Zucker DS. *X-Ray Form Factor, Attenuation and Scattering Tables (version 2.1).* National Institute of Standards and Technology, Gaithersburg, MD. Originally published as Chantler, C.T., J. Phys. Chem. Ref. Data 29(4), 597-1048 (2000); and Chantler, C.T., J. Phys. Chem. Ref. Data 24, 71-643 (1995) (2005). http://www.physics.nist.gov/PhysRefData/FFast/Text/cover.html.

Cowan PL. *Resonant x-ray Raman scattering from atoms and molecules.* In *Resonant anomalous x-ray scattering*, pages 449 – 471. Elsevier Science V.B., North-Holland (1994).

Cowdrey DR and Preston RD. *Elasticity and microfibrillar angle in the wood of Sitka spruce.* Proc. Roy. Soc. **166** (1966), 245 – 272.

Das R, Mills TT, Kwok LW, Maskel GS, Millett IS, Doniach S, Finkelstein KD, Herschlag D and Pollack L. *Counterion distribution around DNA probed by solution x-ray scattering.* Phys. Rev. Lett. **90(18)** (2003), 188103.

Dingenouts N, Merkle R, Guo X, Narayanan T, Goerigk G and Ballauff M. *Use of anomalous small-angle x-ray scattering for the investigation of highly charged colloids.* J. Appl. Cryst. **36(3)** (2003), 578 – 582.

Donaldson LA and Burdon RD. *Clonal variation and repeatability of microfibril angle in Pinus radiata.* New Zealand Journal of Forestry Science **25(2)** (1995), 164 – 174.

Dong D and Fricke AL. *Intrinsic viscosity and molecular weight of kraft lignin.* Polymer **36(10)** (1995), 2075 – 2078.

Eissen M, Metzger JO, Schmidt E and Scheidewind U. *10 years after Rio—Concepts on the contribution of chemistry to sustainable development.* Angew. Chem. Int. Ed. **41(3)** (2002), 414 – 436.

Elliott SR. *Physics of amorphous materials.* Longman group Limited, London (1984).

Evans G and Pettifer RF. *CHOOCH: a program for deriving anomalous-scattering factors from X-ray fluorescence spectra.* J. Appl. Crystallogr. **34(1)** (2001), 82 – 86.

Feigin LA and Svergun DI. *Structure Analysis by Small-Angle X-Ray and Neutron Scattering.* Plenum Press, New York (1987).

Furano H, Takano T, Hirosawa S, Kamitakahara H and Nakatsubo F. *Chemical structure elucidation of total lignins in woods. Part II: Analysis of a fraction of residual wood left after MWL isolation and solubilized in lithium chloride/N,N-dimethylacetamide.* Holzforschung **60** (2006), 653 – 658.

Gardon JL and Mason SG. *Physicochemical studies of ligninsulphonates. II. Behaviour as polyelectrolytes.* Can. J. Chem. **33** (1955), 1491 – 1501.

Gellerstedt G. *The reactions of lignin during sulfite pulping.* Svensk papperstidning **16** (1976), 537 – 543.

Glatter O and Kratky O, editors. *Small Angle X-ray scattering.* Academic Press, London (1982).

Goerigk G, Haubold HG, Lyon O and Simon JP. *Anomalous small-angle x-ray scattering in materials science.* J. Appl. Cryst. **36(3)** (2003), 425 – 429.

Goring DIA. *Thermal softening of lignin, hemicelluloses and cellulose.* Pulp Pap. Mag. Can. **64** (1963), T517 – T527.

Gosselink RJA, de Jong E, Guran B and Abärlich A. *Co-ordination network for lignin — standardisation, production and applications adapted to market requirements (EUROLIGNIN).* Ind. Crop. Prod. **20** (2004), 121 – 129.

Goudeau P, Fontaine A, Naudon A and Williams CE. *Anomalous small-angle x-ray scattering in metallurgy: a feasibility experiment with an Al-Zn alloy.* J. Appl. Cryst. **19** (1986), 19 – 24.

Guinier A. *X-ray Diffraction. In Crystals, Imperfect Crystals, and Amorphous Bodies.* Dover publications, Inc., New York (1994).

Guinier A and Fournet G. *Small-angle scattering of x-rays.* John Wiley & Sons, New York (1955).

Gundersen SA, Sæther Ø and Sjöblom J. *Salt effects on lignosulfonate and Kraft lignin stabilized O/W-emulsions studied by means of electrical conductivity and video-enhanced microscopy.* Colloids Surf., A **186** (2001), 141–153.

Hansen JP and Hayter JB. *A rescaled MSA structure factor for dilute charged colloidal dispersions.* Mol. Phys. **46(3)** (1982), 651 – 656.

Haubold HG, Gebhardt R, Buth G and Goerigk G. *Structural characterization of compositional and density inhomogeneities by ASAXS.* In *Resonant anomalous x-ray scattering*, pages 295 – 304. Elsevier Science V.B., North-Holland (1994).

Hayter JB and Penfold J. *An analytical structure factor for macroion solutions.* Mol. Phys **42(1)** (1981), 109 – 118.

Hayter JB and Penfold J. *Determination of micelle structure and charge by neutron small-angle scattering.* Colloid. Polym. Sci. **261** (1983), 1022 – 1030.

He J, Kunitake T and Nakao A. *Facile in situ synthesis of noble metal nanoparticles in porous cellulose fibers.* Chem. Mater. **15(23)** (2003), 4401 – 4406.

Hendrickson WA. *Determination of macromolecular structures from anomalous diffraction of synchrotron radiation.* Science **254(5028)** (1991), 51 – 58.

Hori R, Müller M, Lichtenegger UWHC, Fratzl P and Sugiyama J. *The importance of seasonal differences in the cellulose microfibril angle in softwoods in determining acoustic properties.* J. Mater. Sci. **37** (2002), 4279 – 4284.

Hori R and Wada M. *The thermal expansion of wood cellulose crystals.* Cellulose **12** (2005), 479 – 484.

Hori R and Wada M. *The thermal expansion of cellulose II and III_{II} crystals.* Cellulose **13** (2006), 281 – 290.

Horkay F, Hecht AM, Rochas C, Basser PJ and Geissler E. *Anomalous small angle x-ray scattering determination of ion distribution around a polyelectrolyte biopolymer in salt solution.* J. Chem. Phys. **125(3)** (2006), 234904.

Huang TC, Toraya H, Blanton TN and Wu Y. *X-Ray powder diffraction analysis of silver behenate, a possible low-angle diffraction standard.* J. Appl. Crystallogr. **26** (1993), 180 – 184.

Hunter RJ. *Foundations of Colloid Science*, vol. I. Clarendon press, Oxford, 2nd ed. (1991).

Hunter RJ. *Foundations of Colloid Science*, vol. II. Clarendon press, Oxford, 3rd ed. (1992).

Irvine M. *The glass transition of lignin and hemicellulose and their measurement by differential thermal analysis.* Tappi J. **67(5)** (1984), 118 – 121.

Jurasek L. *Morphology of Computer-Modeled Lignin Structures: Fractal Dimensions, Orientation and Porosity.* J. Pulp Paper Sci. **22(10)** (1996), J376 – J380.

Karmanov AP and Monakov YB. *The structure of lignin macromolecules.* Vysokomolekulyarnye soedineniya seriya A & seriya B **38(6)** (1996), 1631 – 1642. In Russian.

Kim DY, Nishiyama Y, Wada M, Kuga S and Okano T. *Thermal decomposition of cellulose crystallites in wood.* Holszforschung **55** (2001), 521 – 524.

Kinning DJ and Thomas EL. *Hard-sphere interactions between spherical domains in diblock copolymers.* Macromolecules **17** (1984), 1712 – 1718.

Klemm D, Heublein B, Fink HP and Bohn A. *Cellulose: Fascinating biopolymer and sustainable raw material.* Angew. Chem. Int. Ed. **44** (2005), 3358 – 3393.

Kline SR. *Reduction and analysis of SANS and USANS data using Igor Pro.* J. Appl. Cryst. **39** (2006), 895 – 900.

Klug HP and Alexander LE. *X-ray diffraction procedures.* John Wiley & Sons, New York, 2nd ed. (1974).

Langan P, Sukumar N, Nishiyama Y and Chanzy H. *Synchrotron x-ray structures of cellulose I_β and regenerated cellulose II at ambient temperature and 100 K.* Cellulose **12** (2005), 551 – 562.

Lawoko M, Henriksson G and Gellerstedt G. *Characterization of lignin-carbohydrate complexes from spruce sulfite pulp.* Holzforschung **60** (2006), 162 – 165.

Li Y, Mlynár J and Sarkanen S. *The first 85% Kraft lignin-based thermoplastics.* J. Polym. Sci., Part B: Polym. Phys. **35** (1997), 1899–1910.

Lindström T. *The colloidal behaviour of kraft lignin. Part I.: Association and gelation of kraft lignin in aqueous solutions.* Colloid Polym. Sci. **257** (1979), 277 – 285.

Lora JH and Glasser WG. *Recent industrial applications of lignin: A sustainable alternative to nonrenewable materials.* J. Polym. Environ. **10** (2002), 39 – 48.

Ludwig Jr KF. *Anomalous x-ray scattering studies of liquids*. Ph.D. thesis, Stanford University (1986).

Lyttle FW. *The EXAFS family tree: a personal history of the development of extended X-ray absorption fine structure*. J. Synchrotron Rad. **6** (1999), 123 – 134.

Mafé S, Manzanares JA, Kontturi AK and Kontturi K. *Temperature effects on counterion binding to spherical polyelectrolytes: the charge-discharge transition of lignosulfonate*. Bioelectrochem. Bioenerg. **38** (1995), 367 – 375.

Martin JE and Hurd AJ. *Scattering from fractals*. J. Appl. Cryst. **20** (1987), 61 – 78.

Maximova N. *Adsorption of lignin and lignin/cationic polymer complexes on cellulose fibres and their effect on sheet properties*. Ph.D. thesis, Helsinki University of Technology (2004).

Mecke A, Lee I, Baker Jr JR, Banaszak Holl MM and Orr BG. *Deformability of poly(amidoamine) dendrimers*. Eur. Phys. J. E **15** (2004), 7 – 16.

Merkle G, Auerbach S, Burchard W, Lindner A and Wegener G. *Light scattering of acetylated lignin*. J. Appl. Polym. Sci. **45** (1992), 407 – 415.

Merritt EA. *X-ray Anomalous Scattering*. http://skuld.bmsc.washington.edu/ ... scatter/AS_index.html (2003). Calculated using Cromer–Liberman theory.

Müller M, Burghammer M and Sugiyama J. *Direct investigation of the structural properties of tension wood cellulose microfibrils using microbeam x-ray fibre diffraction*. Holzforschung **60** (2006), 474 – 479.

Myszewski JH, Bridgwater FE, Lowe WJ, Byram TD and Megraw RA. *Genetic variation in the microfibril angle of loblolly pine from two test sites*. South. J. Appl. For. **28(4)** (2004), 196 – 204.

Nadif A, Hunkeler D and Käuper P. *Sulfur-free lignins from alkaline pulping tested in mortar for use as mortar additives*. Bioresour. Technol. **84** (2002), 49 – 55.

Nishiyama Y, Langan P and Chanzy H. *Crystal structure and hydrogen-bonding system in cellulose I_β from synchrotron x-ray and neutron fiber diffraction*. J. Am. Chem. Soc. **124** (2002), 9074 – 9082.

Nishiyama Y, Sugiyama J, Chanzy H and Langan P. *Crystal structure and hydrogen bonding system in cellulose I_α from synchrotron x-ray and neutron fiber diffraction*. J. Am. Chem. Soc. **125** (2003), 14300 – 14306.

NIST. *http://www.ncnr.nist.gov/programs/sans/data/red_anal.html* (2006).

Norgren M, Edlund H and Wågberg L. *Aggregation of Lignin Derivatives under Alkaline Conditions. Kinetics and Aggregate Structure*. Langmuir **18** (2002), 2859 – 2865.

Norgren M, Edlund H, Wågberg L, Lindström B and Annergren G. *Aggregation of kraft lignin derivatives under conditions relevant to the process, part I: phase behaviour*. Colloids Surf. A **194** (2001), 85 – 96.

Orthaber D, Bergmann A and Glatter O. *SAXS experiments on absolute scale with Kratky systems using water as a secondary standard.* J. Appl. Crystallogr. **33** (2000), 218 – 225.

Ottewill RH, Rennie AR and Johnson GDW. *Small-angle neutron scattering studies on binary mixtures of polystyrene and perfluorinated particles.* Adv. Colloid Interface Sci. **100 – 102** (2003), 585 – 611.

Ouyang X, Qiu X and Chen P. *Physicochemical characterization of calcium lignosulfonate – A potentially useful water reducer.* Colloids Surf., A **282 – 283** (2006), 489 – 497.

Pasquini D, Balogh DT, Antunes PA, Constantino CJL, Curvelo AAS, Aroca RF and Oliviera Jr ON. *Surface morphology and molecular organization of lignins in Langmuir-Blodgett films.* Langmuir **18** (2002), 6593 – 6596.

Pedersen JS. *Analysis of small-angle scattering data from colloids and polymer solutions: modeling and least-squares fitting.* Adv. Colloid Interface Sci. **70** (1997), 171 – 210.

Petrus L and Noordermeer MA. *Biomass to biofuels, a chemical perspective.* Green chemistry **8(10)** (2005), 861 – 867.

Peura M, Müller M, Serimaa R, Vainio U, Sarén MP, Saranpää P and Burghammer M. *Structural studies of single wood cell walls by synchrotron x-ray microdiffraction and polarised light microscopy.* Nucl. Instrum. Methods Phys. Res., Sect. B **238** (2005), 16 – 20.

Philips EWJ. *The inclination of the fibrils in the cell wall and its relation to the compression strength of timber.* Empire Forestry Journal **20** (1941), 74 – 78.

Picker KM and Hoag SW. *Characterization of the thermal properties of microcrystalline cellulose by modulated temperature differential scanning calorimetry.* J. Pharm. Sci. **91(2)** (2002), 342 – 349.

Preston RD. *The Physical Biology of Plant Cell Walls.* Chapman and Hall, London (1974).

Pye EK. *Biorefining; a major opportunity for the sugar cane industry.* International Sugar Journal **107(1276)** (2005), 222 – 230.

Radotić K, Mićić M and Jeremić M. *New insights into the structural organization of the plant polymer lignin.* Ann. N. Y. Acad. Sci. **1048** (2005), 215 – 229.

Radotić K, Tasić M, Jeremić M, Budimlija Z, Simić-Krstić J, Polzović A and Bolžović Z. *Fractal Analysis of STM Images of Lignin Polymer Obtained by in vitro Synthesis.* Gen. Physiol. Biophys. **19** (2000), 171–180.

Raghuraman A, Tiwari V, Thakkar JN, Gunnarsson GT, Shukla D, Hindle M and Desai UR. *Structural characterization of a serendipitously discovered bioactive macromolecules, lignin sulfate.* Biomacromolecules **6** (2005), 2822 – 2832.

Rehr JJ. *Theory and calculations of x-ray spectra: XAS, XES, XRS, and NRIXS.* Radiat. Phys. Chem. **75(11)** (2006), 1547 – 1558.

Saalwächter K, Burchard W, Klüfers P, Kettenbach G, Mayer P, Klemm D and Dugarmaa S. *Cellulose solutions in water containing metal complexes.* Macromolecules **33** (2000), 4094 – 4107.

Sarén MP. *Characterisation of properties of coniferous wood tracheids by x-ray diffraction, laser scattering and microscopy.* Ph.D. thesis, University of Helsinki (2006). http://ethesis.helsinki.fi/en/.

Sarkanen KV and Ludwig CH, editors. *Lignins: Occurrence, Formation, Structure and Reactions.* Wiley-Interscience, New York (1971).

Schmidt PW. *Use of scattering to determine the fractal dimension.* In D Avnir, editor, *Fractal Approach to Heterogeneous Chemistry.* John Wiley & Sons (1989).

Schmidt PW. *Small-angle scattering studies of disordered, porous and fractal systems.* J. Appl. Cryst. **24(5)** (1991), 414 – 435.

Scott G and Wiles DM. *Programmed-life plastics from polyolefins: A new look at sustainability.* Biomacromolecules **2(3)** (2001), 615 – 622.

Seitsonen S and Mikkonen I. *X-ray study on the thermal transition of cotton cellulose.* Polym. J. **5(3)** (1973), 263 – 267.

Shen SH, Sheu EY, Kallus J and Hoffmann H. *Small-angle neutron scattering investigation of correlations in charged macromolecular and supramolecular solutions.* J. Appl. Crystallogr. **21** (1988), 751 – 769.

Simola LK, Lemmetyinen J and Santanen A. *Lignin release and photomixotrophism in suspension cultures of Picea abies.* Physiol. plant. **84** (1992), 374–379.

Simon JP and Lyon O. *Anomalous small angle x-ray scattering in materials science.* In *Resonant anomalous x-ray scattering*, pages 305 – 322. Elsevier Science V.B., North-Holland (1994).

Sjöström E. *Wood Chemisty: Fundamentals and Applications.* Academic press, San Diego (1993).

Spalla O, Lyonnard S and Testard F. *Analysis of the small-angle intensity scattered by a porous and granular medium.* J. Appl. Cryst. **36** (2003), 338 – 347.

Stamm AJ and Hansen LA. *Bonding force of cellulosic materials for water (from specific volume and thermal data).* J. Phys. Chem. **41** (1937), 1007–1016.

Sugiyama J, Vuong R and Chanzy H. *Electron diffraction study on the two crystalline phases occuring in native cellulose from algal cell wall.* Macromolecules **24** (1991), 4168 – 4175.

Suzuki T and Nakagami H. *Effect of crystallinity of microcrystalline cellulose on the compactability and dissolution of tablets.* Eur. J. Pharm. Biopharm. **47** (1999), 225 – 230.

Svergun DI. *Mathematical methods in small-angle scattering data analysis.* J. Appl. Cryst. **24** (1991), 485 – 492.

Svergun DI and Koch MJ. *Small-angle scattering studies of biological macromolecules in solution*. Rep. Prog. Phys. **66** (2003), 1735 – 1782.

Takahashi M and Takenaka H. *X-ray study of thermal expansion and transition of crystalline cellulose*. Polym. J. **14(9)** (1982), 675 – 679.

Thompson D. personal communication (2006). Contact person for the Coillte Research Station.

Treacy M, Evertsen J and Ní Dhubháin A. *A comparison of the mehcanical and physical wood properties of a range of Sitka spruce provenances*. Tech. rep., National council for Forest Research & Development COFORD (2000).

Vainio U, Serimaa R and Gravitis J. *X-ray scattering methods in the study of soft materials*. Latvian Journal of Physics and Technical Sciences **2006(4)** (2006), 14 – 24.

Vainio U, Serimaa R, Gravitis J and Hortling B. *Fractal dimensions of extracted lignins at elevated temperatures by small-angle x-ray scattering*. In *Proceedings of the Seventh European Workshop on Lignocellulosics and Pulp*. Turku, Finland (2002).

Vrij A. *Mixtures of hard spheres in the Percus-Yevick approximation. Light scattering at finite angles*. J. Chem. Phys. **71(8)** (1979), 3267 – 3270.

Wada M, Chanzy H, Nishiyama Y and Langan P. *Cellulose III_I crystal structure and hydrogen bonding by synchrotron x-ray and neutron fiber diffraction*. Macromolecules **37** (2004a), 8548 – 8555.

Wada M, Heux L and Sugiyama J. *Polymorphism of cellulose I family: reinvestigation of cellulose IV_I*. Biomacromolecules **5** (2004b), 1385 – 1391.

Wallberg O and Jönson AS. *Separation of lignin in kraft cooking liquor from a continuous digester by ultrafiltration at temperature above 100°C*. Desalination **195** (2006), 187–200.

Watanabe A, Morita S and Ozaki Y. *Temperature-dependent structural changes in hydrogen bonds in microcrystalline cellulose studied by infrared and near-infrared spectroscopy wih perturbation-correlation moving-window two-dimensional correlation analysis*. Appl. Spectrosc. **60(6)** (2006), 611 – 618.

Wilson AJC, editor. *International tables for crystallography*, vol. C: Mathematical, physical and chemical tables. Kluwer academic publishers for The International Union of Crystallography, Dordrecht, 1st ed. (1995).

Zhu S, Wu Y, Chen Q, Yu Z, Wang C, Jin S, Ding Y and Wu G. *Dissolution of cellulose with ionic liquids and its application: a mini-review*. Green chem. **8** (2006), 325 – 327.

Zugenmaier P. *Conformation and packing of various crystalline cellulose fibers*. Prog. Polym. Sci. **26** (2001), 1341 – 1417.